INVESTIGATION OF THE EFFECTS OF STRUCTURAL NONLINEARITIES ON THE AEROELASTIC STABILITY OF TWO-DIMENSIONAL AIRFOIL

İKİ BOYUTLU KANAT KESİTLERİNDE YAPISAL DOĞRUSALSIZLIKLARIN AEROELASTİK KARARLILIĞA ETKİLERİNİN İNCELENMESİ

OĞUZHAN KOCA

PROF. DR. SELAHATTİN ÇAĞLAR BAŞLAMIŞLI
Supervisor

Submitted to

Graduate School of Science and Engineering of Hacettepe University

as a Partial Fulfillment to Requirements

for the Award of the Degree of MASTER OF SCIENCE

in Mechanical Engineering

2022

ABSTRACT

INVESTIGATION OF THE EFFECTS OF STRUCTURAL NONLINEARITIES ON THE AEROELASTIC STABILITY OF TWO DIMENSIONAL AIRFOIL

Oğuzhan KOCA

Master of Science, Mechanical Engineering Department

Supervisor: Prof. Dr. Selahattin Çağlar BAŞLAMIŞLI

February 2022, 81 pages

In this thesis, the effects of nonlinear structural components on the aeroelastic stability of a 2D airfoil section which is studied in the academic and industrial environments since the theoretical foundation that was published in 1940s, is investigated. The aerodynamic forces obtained from the potential flow theory were used in the studies. Potential flow theory is decided to be used in this thesis as it is a widely used in aeroelastic studies hence it gives successful results at subsonic speeds and can be applied mathematically quickly and simply. The time integration methods are found to be time inefficient especially at higher airspeed where the oscillation amplitudes are high as well. It is also realized that time integration methods are not capable of describing the stability and bifurcations in details. For these reasons, numerical continuation methods are decided to be used to obtain detailed stability and bifurcation characteristics of the system in shorter times. The flutter speed of the linear system is found with solving eigenvalue problem which is derived from equation of motion. Again using this equations and mathematical expressions of the nonlinear structural components, the nonlinear differential equations were obtained. The nonlinear

structural components cubic stiffness, quadratic damping and free-play are studied in this thesis. The numerical continuation analyzes are performed in an open source MATLAB package software MATCONT. In these analyzes, it was observed that the nonlinear components have important impact on the stability of the system and caused to arise limit cycle oscillations. It is also found that, the stability and amplitude of the limit cycle oscillations are highly effected from the coefficients of nonlinear components and the degree of freedom where the nonlinear components are introduced.

Keywords: aeroelasticity, flutter, limit cycle oscillation, bifurcation, dynamic stability, numerical continuation

ii

ÖZET

İKİ BOYUTLU KANAT KESİTLERİNDE YAPISAL DOĞRUSALSIZLIKLARIN AEROELASTİK KARARLILIĞA ETKİLERİNİN İNCELENMESİ

Oğuzhan KOCA

Yüksek Lisans, Makine Mühendisliği Bölümü

Tez Danışmanı: Prof. Dr. Selahattin Çağlar BAŞLAMIŞLI

Şubat 2022, 81 sayfa

Sunulan bu tezde, mühendisliğin hem akademik hem de endüstriyel alanlarında teorik temellerinin atıldığı 1940'lı yıllardan bu yana üzerinde çalışılmaya devam edilen iki boyutlu kanat kesitlerinde bulunan doğrusal olmayan yapısal etkilerin aeroelastik kararlılığa etkisi incelenmiştir. Yapılan çalışmalarda potansiyel akış teorisinden elde edilen aerodinamik kuvvetler kullanılmıştır. Potansiyel akış teorisi, ses altı hızlarda başarılı sonuçlar vermesi ve matematiksel olarak hızlı ve basit bir şekilde uygulanabilir olması nedeniyle aeroelastik çalışmalarda oldukça yaygın olarak kullanılan bir metot olması dolayısıyla bu tezde de kullanılmasına karar verilmiştir. Doğrusal olmayan yapısal bileşenlerin etkilerinin incelemelerde doğrusal olmama seviyelerinin yüksek olduğu durumlarda özellikle yüksek hava hızları için artan genliklerle beraber zaman integrasyon metotları ile çözümlerin uzun sürdüğü, sistem kararlılığı ve bifurkasyonların detaylı olarak kestirilemediği gözlenmiştir. Bu sebeple nümerik devamlılık metotları kullanılarak daha hızlı çözümler alınması ve de sistem karakteristiğinin daha detaylı belirlenmesi hedeflenmiştir. Hareket denklemlerinden elde edilen özdeğer problemi çözülerek doğrusal

sistemin çırpıntı hızı belirlenmiştir. Yine bu denklemlere doğrusal olmayan yapısal bileşenler eklenerek doğrusal olmayan hareket denklemleri türetilmiştir. Bu tezde incelenen doğrusal olmayan yapısal etkiler; kübik katılık, ikinci derece sönüm ve de boşluklardır. Nümerik devamlılık analizleri açık kaynak bir MATLAB paket programı olan MATCONT ile gerçekleştirilmiştir. Gerçekleştirilen analizler kapsamında doğrusal olmayan bu yapısal bileşenlerin sistemin kararlılığında önemli değişikliklere sebep olduğu ve limitli döngü titreşimlerini oluşturduğu gözlenmiştir. Limitli döngü titreşimlerinin kararlılığının ve genliğinin doğrusal olmayan yapısal bileşenlerin katsayılarına, bu bileşenlerin hangi serbestlikte tanımlandığına göre önemli ölçüde etkilendiği görülmüştür.

Anahtar Kelimeler: aeroelastisite, çırpıntı, limit döngü titreşimi, bifurkasyon, dinamik kararlılık, nümerik devamlılık

ACKNOWLEDGEMENTS

TABLE OF CONTENTS

LIST OF TABLES

LIST OF FIGURES

xi

SYMBOLS AND ABBREVIATIONS

Symbols

h   Displacement in plunge direction

a   Rotation in pitching direction

b   Rotation about control surface hinge axiss

U   Airspeed

δ   Free-play angle

K_h Stiffness in plunge direction

K_α Stiffness in pitching direction

K_β Stiffness value of control surface hinge

Abbreviations

LCO   Limit Cycle Oscillations

EOM   Equation of Motion

AEOM   Aeroelastic Equation of Motion

NS   Neimark-Sacker

LPC   Limit Point of Cycles

BPC   Branch Point of Cycles

PD   Period Doubling

BPC   Branch point

H   Hopf

1. INTRODUCTION

In aviation, the field of aeroelasticity gain importance with the higher speed demands for aircrafts. This demand was the main design parameter for the aircrafts both structurally and geometrically. The new designs were converging to the thin aircrafts with less mass and more powerful engines and these types of aircrafts started to show certain characteristic or motion which can be static or dynamic. The aerodynamic forces also changed with the speed of aircrafts and the geometry.

Aeroelasticity investigates the interaction of the fluid and structure. The interactions could be seen in details in Figure 1.1. Aeroelastic behavior could be divided into two main branches which are static aeroelasticity and dynamic aeroelasticity. For calculation of static aeroelasticity, the elastic and aerodynamic forces must be included in mathematical model. However, in dynamic aeroelasticity inertial forces must be involved too.
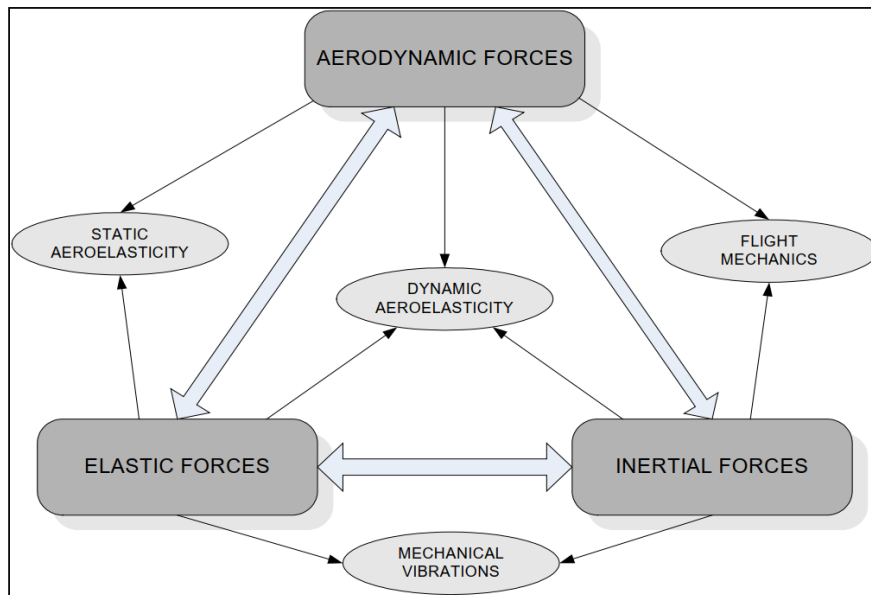
Figure 1.1. Interactions between field of elasticity, dynamics and aerodynamic [1].

Static and dynamic aeroelasticity also have branches. The branches of the static aeroelasticity are control reversal, divergence, control effectiveness. Dynamic aeroelasticity

can be investigated in following phenomena; flutter, buffeting, buzzing, dynamic response. All these aeroelastic phenomena are briefly explained.

1.1.   Static Aeroelasticity

One of the first aeroelastic failures was the reason of restoring elastic forces could not compensate the aerodynamic forces. This inequality of the moment on the wing causes large deformation at a certain airspeed limit and the failure occurs. This type of failure is called divergence. Generally, the early era thin winged war planes were prone to divergence. Divergence is not caused by vibrations so it is not a dynamic behavior.

In aircrafts, swept angle of the wing changes the occurrence condition of instability as can be seen in Figure 1.2. The reason for the lower divergence speed of forward swept wing is the twisting effects due to aerodynamic loading. On the contrary, the deformation of back-swept wing is more likely to be bending.
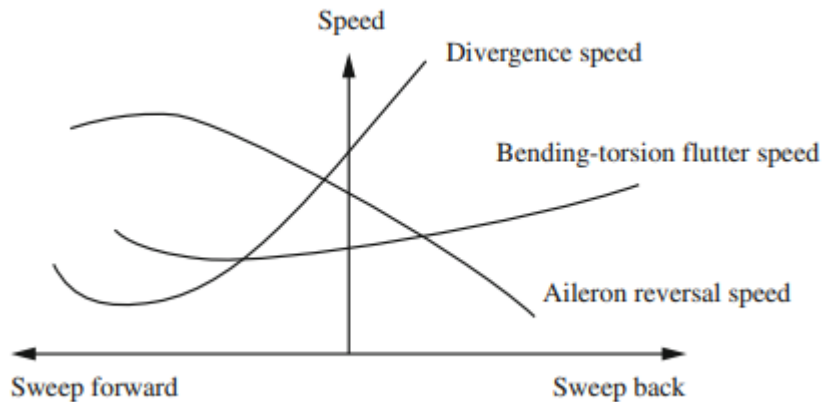
Figure 1.2. Effects of swept angle on aeroelastic response [2].

Aileron effectiveness is one another subject of the static aeroelasticity. The locations of the aerodynamic and the elastic centers of the airfoil section have effect on lift, moment and also controllability of the air vehicle. In steady state condition, if the aerodynamic and elastic centers coincide, the total forces on the wing would not create moment. However, the deformation of the wing will change the location of aerodynamic center. So, the total

forces will create moment on the wing. For example, the down moving control surface causes to translation of aerodynamic pressure center to backwards. It means that the total aerodynamic force will create moment around elastic axis. This moment will cause a downward motion on the leading edge. It will also cause both the effective angle of attack and total lift force to decrease. The decrease on the total lift is called as reduced control surface effectiveness. At a certain speed, the aileron inputs will not be able to perform accordingly but will cause opposite of the desired inputs. This situation is called as aileron or control-surface reversal.

1.2.   Dynamic Aeroelasticity

As it is shown in Figure 1.1, dynamic aeroelasticity is a field that investigates inertial, aerodynamic and elastic forces. In all aeroelastic phenomena, the flutter is the most important one due to its catastrophic results. The flutter term is used for defining unstable behavior of the structure at specific speed and altitude. In flutter, the structure deforms under unsteady aerodynamic forces which leads to change in the total lift area. This change causes another deformation field and this situation goes on and on. These cycles of event will repeat itself while the total damping of the system is greater than zero. The meaning of being damping ratio of a system is greater than zero is the total energy is no longer in the system in mechanical form. Otherwise, if the total damping ratio is less than zero, the system will start to extract energy from the air which will cause amplifying the amplitude of the vibration. At a certain point the amplitude of the vibration will exceed the limits and cause failure. Also, if the total damping equals zero, it is possible to see limit cycles in the system. In general, flutter occurred mostly in the linear systems and LCO occurred in nonlinear systems. In the context of nonlinear system theory, an LCO is one of the simplest bifurcations, and defined as 'first stop on the road to chaos' [3]. In LCO, the total damping ratio of the system is not less than zero but equals to zero. This equivalence causes the fixed amplitude oscillations. The amplitude of oscillations generally depends on the amount of the nonlinearity and initial conditions. At a specific speed, the LCO may turn in to flutter. It should be easier to understand and visualize the response of a structure with respect to changing speed. The responses of a missile control fin are given in the Figure 1.3. One can see that at 200 m/s speed the response of the fin is damped out. At 213 m/s the

response is first damped out after a second the amplitude of the response starts to increase to a limit. In the third figure, at 233 m/s, the vibration is damped out to a certain level after that LCO is not damped out. Finally in the last figure, the speed increases to 234 m/s and the amplitude of the vibration increases to very high levels, this behavior is called flutter.
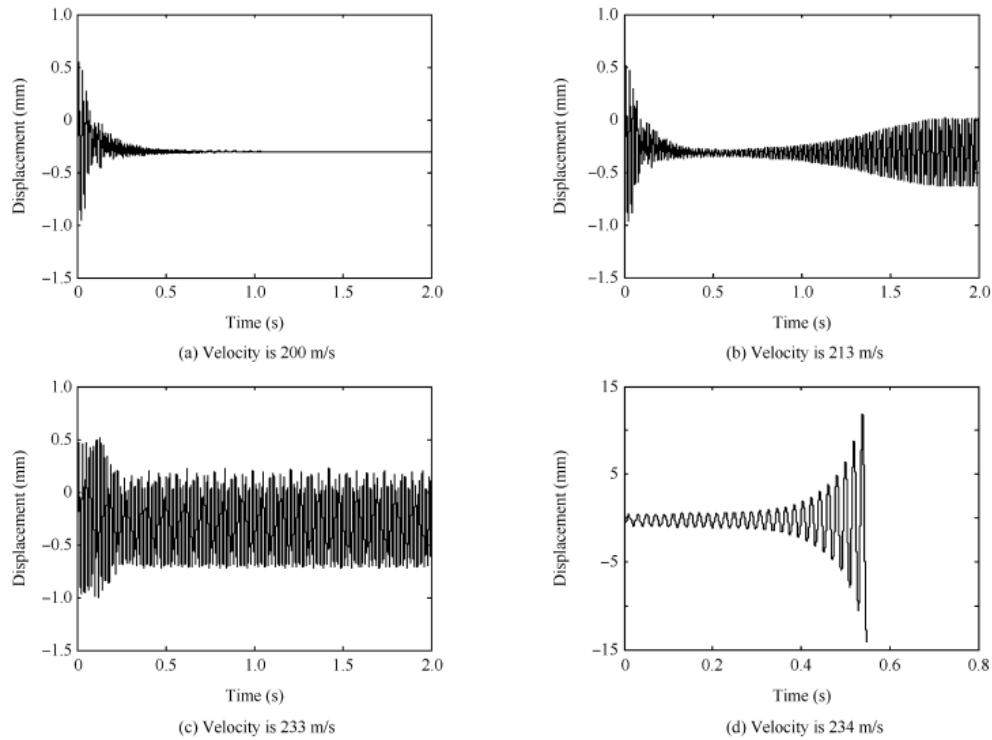
Figure 1.3. The responses of a missile fin at different air speeds [4].

In flutter, the system extracts energy from air via modal coupling. The flutter cannot be occurred unless there are contributions from two modes. The well-known modal couplings for an aircraft are listed below:

- Classic flutter, wing bending – wing torsion coupling
- Body flutter, wing torsion – body pitching coupling
- Control surface coupling, control surface rotation – wing bending

4
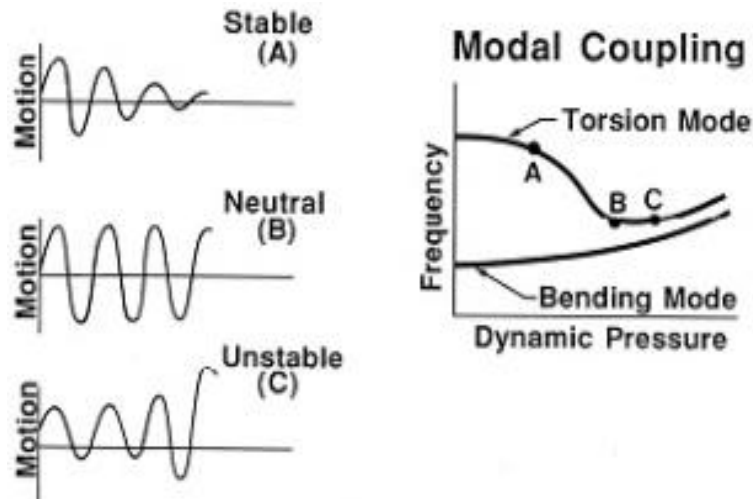
Figure 1.4. Modal coupling [5]

Separately neither motion causes flutter. At critical values of amplitude and phase angle, the forces produced by one motion excite the other; the two types of motion are then said to be coupled. As can be seen in Figure 1.4, the frequencies of the modes are getting closer while the dynamic pressure increases.

At transonic speeds, another important phenomenon, buffeting occurs due to flow separation and shock induced wakes. High performance aircrafts like F-16, F-15 and F-18 show buffeting generally at high angle of attack maneuvers. As indicated in MIL-STD-810G buffeting usually happens in the interval of 10-50 Hz in the form of random vibration. The flow separation from the wing, control surfaces, nacelles, wing-pylon junctions may induce loading at tail and stabilizers. The loading may cause fatigue on the aircraft parts. In general tails are vulnerable to buffeting [6].

Figure 1.5. Tail buffeting of F-18 [7]

It is mentioned that in common flutter must occur as coupling of at least two modes of the structure. As oppose to this explanation there is also single degree of freedom which is called control surface buzz or just buzz flutter. In this type of aeroelastic phenomena the control surface oscillates around its hinge due to location of aerodynamic shock in transonic or low supersonic region.

The failures are not only concerns of aeroelasticity. It is also used in calculating dynamic response of maneuver loads, gust, landing loads and taxi operations. These calculations are grouped under the term of dynamic response.

1.3.   Historical Background

The first examples of solution for the aeroelastic problems date back to several centuries ago in Holland. The location of the wind mill blade spar was moved from middle of the chord to one quarter of the chord where aerodynamic center is located. This modification made in order to prevent twisting moment around elastic axis [8].

6

In early years of aviation, aeroelasticity based designs, calculations or problems were studied in many projects like Wright Brothers, Langley's tandem monoplane etc. In Wright Brothers case, they used wing-warp method to control roll of the plane [9]. The Wright brothers patented their invention, all aircraft control tools were covered with this patent. The wing-warp method was controlled by the pilot easily and creates rolling moment around the center of the fuselage.
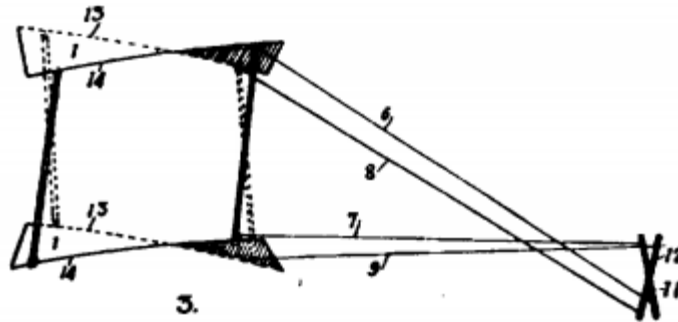
Figure 1.6. Wright Brothers' aeroelastic model. [9]

Aside from the wing-warp method, Wright brothers also studied on propellers, and they found out that thinning propeller caused thrust loss due to structural deformation and angle change.

Another example for early aeroelastic problem is Langley's monoplane. Professor Samuel P. Langley of the Smithsonian Institute designed an airdrome. Langley's monoplane was launched from catapult mechanism nine days before the Wright brothers' flight. The reason behind the failure will be explained as the divergence which is a static phenomenon related with the torsional strength of the wing structure. As in cited in Glenn's article, after some modification on Langley's monoplane, it succeeded to fly at a short distance. These modifications aimed to strengthen the wing structure to prevent change of angle of attack and center of pressure which causes divergence [10].
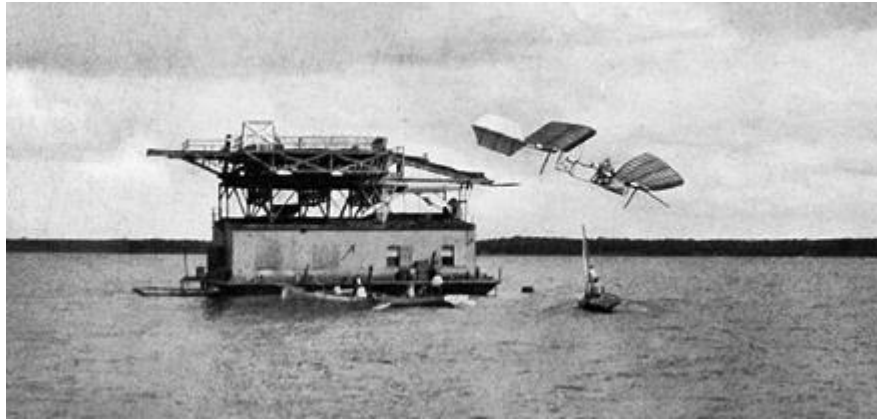
Figure 1.7. Launch of Langley's monoplane

During the World War I, both sides suffered from aeroelastic problems, mostly flutter and divergence caused losses. In England, E. W. Lanchester studied on the excess vibration on the tail of a bomber, Handley Page O/400. He explained the reason as the vibration due to insufficient stiffness in torsional direction because the elevators of the airplane were independent from each other, and was controlled separately by the wires. He also described the nature of the vibration as; the vibrations were not the results of any source of forced excitation but self-excited. He came with the idea of torque tube to eliminate the excess vibrations. The same solution was applied to another plane, Havilland DH-9. Brostow and Fage theoretically backed up the Lanchester's solution on Handley Page's torque tube. Later, the torque tube became basic design methodology.

The aeroelastic problems became more frequent and visible, when the monoplane era started. The biplane wings had higher torsional rigidity due to bracing. The monoplanes had many issues in the context of instabilities like flutter, divergence, control surface reversal and ineffectiveness due to insufficient torsional rigidity. One of the early victims of the monoplane design was Fokker D-8. The plane had a cantilever wing design and its torsional rigidity was determined according to the criteria that used in biplane designs. The Fokker D-8 had superior capabilities which were decided to start production. After a few days, many planes had similar wing failures, The Fokker Company and army tried to understand the problem. Static deformation and strength tests were performed to understand the reason of the failure. However, as it is understood the reason was not related with the strength.

Anthony Fokker who discovered the reason try to explain it like that: "I discovered that with the increasing load the angle of incidence at the wing tips increased perceptibly. It sudden dawned on me that this increasing angle of incidence was the cause of the wings collapse, as logically the load resulting from the air pressure in a steep dive would increase faster at the wing tips than at the middle. The resulting torsion caused the wings to collapse under the strain of combat maneuvers." [11]
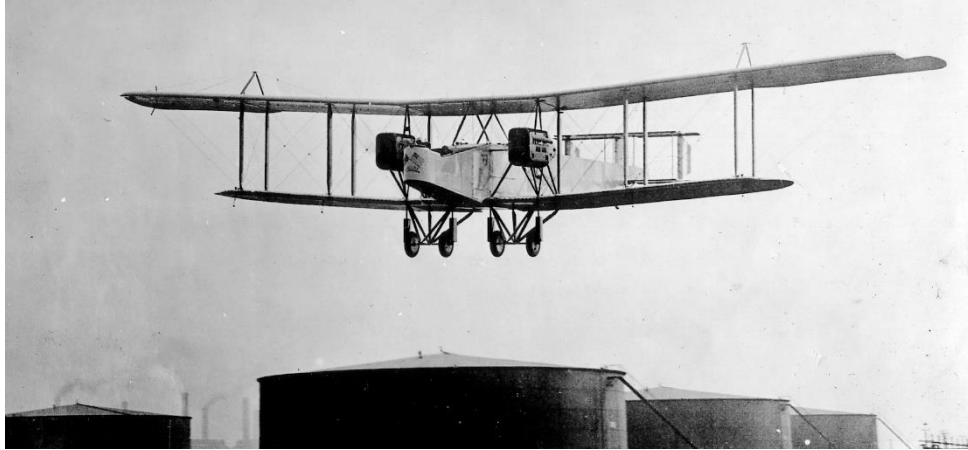
Figure 1.8. Handley Page O/400

Another design to improve both control of the aircraft and the oscillation on the wings applied by the U.S. Army Air Corps to a violent but nondestructive case of wing bending – aileron flutter. The problem was eliminated by applying mass balance method on aileron. In this procedure, the aileron balanced about the aileron hinge line. Baumhaure and Koning were the first ones mentioned about this theorem in 1922 [12].

During the early monoplane era, a lot of failures were recorded and these failures provided understanding on the nature of flutter, divergence, load distribution, aileron effectiveness and aileron reversal. The load distribution and divergence theory was published first by Hans Reissner in 1926 [13]. After six year from Reissner's work, Cox and Pugsley studied aileron reversal and effectiveness and wing divergence [14]. The potential flow theory for the flutter was highly understood and used for design purposes where most of the work was done by Glauert.

In 1925, H. Wagner gave a basic approach to the theoretical problem of non-stationary flow supplementing the harmonic approach in his doctoral thesis. He studied the lift distribution after a sudden change in the angle of incidence or a sudden acquisition of unit downwash.

In 1929, H.G. Küssner published a basic paper on flutter improving Birnbaum's method and was able to converge the problem for $\omega=1.0$ while Birnbaum had convergence issues at the reduced frequencies greater than 0.10. He also investigated the effects of hysteresis/material damping on flutter response.

In 1935, Theodore Theodorsen studied airfoil stability that had plunge, pitch and aileron degrees of freedom. His method created the ability of parametric design and to see the effects of gravity, mass of inertia, mass ratio, and aileron hinge location. In Figure 1.9, it is possible to see the unsteady modeling of Küssner and Wagner which are in time domain and their frequency domain counterparts which are derived from Sears and Theodorsen.
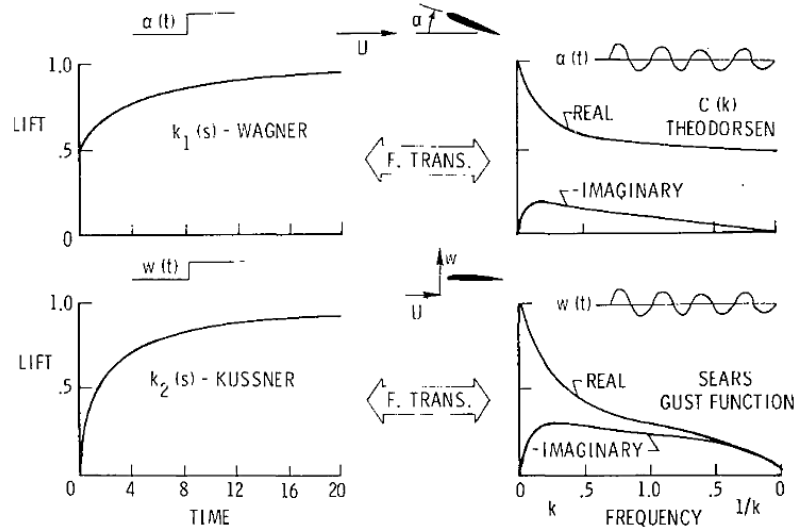
Figure 1.9. Fourier transform relation between time domain and frequency domain modeling methods of unsteady aerodynamics [15].

In 1935, Von Schlippe became the first person who brought a different approach to the flutter testing. The test procedures before Von Schlippe, the pilot dived the aircraft until the

airplane reach to its maximum speed. If there was no failure, the aircraft was clear to fly. Von Sclippe suggested that, while the aircraft was approaching to its flutter speed, the response of the aircraft was showing an asymptotic increase. The flutter speed could be estimated by the position of asymptote and dive could be ceased before the aircraft reach the limits.
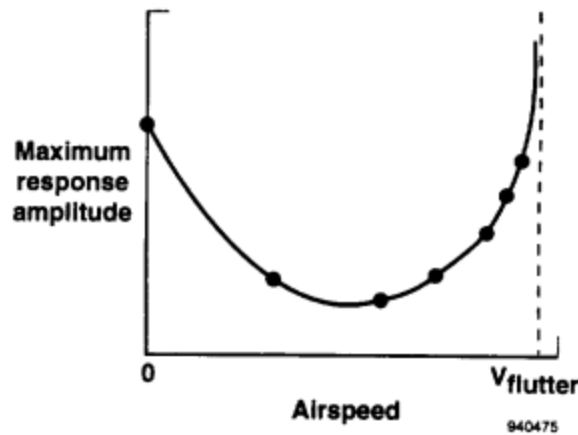
Figure 1.10. Von Schlippe's flight flutter test technique [16]

The effects of structural nonlinearity on aeroelastic response were investigated by Woolston et al. [17] and Shen [18]. They modeled a system with a nonlinear spring and solved via computers. Shen was one the first people who applied harmonic balance method to nonlinear aeroelasticity. The method was first presented by Kryloff and Bogoliuboff [19] and since that method become one of the primary tools for nonlinear dynamics that undergoes periodic oscillations.

The bifurcation theory is used for understanding which parameters cause unstable behavior. In 1994, one of the first studies that apply bifurcation methods to nonlinear aeroelastic systems was presented by Price et al [20]. They used bifurcation diagrams to understand the behavior of typical section with nonlinearity. Nowadays, nonlinear aeroelasticity is an important field for estimating LCO limits, determining design parameters and test planning.

11

1.4. Scope of the Thesis

One of the main aims of this thesis is become acquaintance with the theory of nonlinear aeroelasticity, investigating the effects of nonlinearities that are introduced to a 3DOF airfoil system and the effects of nonlinear parameters on the stability and response of the airfoil with changing airspeed.

1.5. Literature Survey

In this part, previous studies and methods which focused on solving nonlinear aeroelastic problem are going to be summarized. It could be said that the aeroelastic modeling era started with Theodorsen and Garrick [21] as mentioned in historical background part. However, it took ten years to develop structural nonlinear modeling methods [17]. From the very beginning of the first developed model, scientist and engineers are still working on improving better physically representing models. In this thesis many of the previous works were studied and investigated.

The free-play causes sudden changes in stiffness which creates nonlinearity in the system. The linear solution approaches are not valid anymore. The modeling technique for linear aeroelastic stability generally starts with normal mode analysis of the structural model. It is possible to use both frequency domain and time domain methods for modeling aerodynamics. As stated before, Theodorsen and Sear separately were able to model unsteady aerodynamics of an airfoil in frequency domain. The time domain solution of unsteady aerodynamics came from both Küssner and Wagner. The Wagner unsteady aerodynamics is used for 2D modeling of an airfoil.

Modeling 3D structures in time domain requires panel methods such as doublet lattice method (DLM). However, the panel methods cannot be used in time domain analysis directly, since the aerodynamic influence coefficient (AIC) matrix is in frequency domain. It is necessary to represent or approximate the AIC in time domain. This is succeeded through using Rational Function Approximation (RFA) [22], which approximate the AICs obtained from aerodynamic modeling that uses reduced frequency domain.

The nonlinear aeroelasticity could be divided into two such: nonlinear aerodynamic and nonlinear structural properties and physics. The sources in nonlinearity aerodynamics are, turbulence, shock etc. Structural nonlinearity could be classified as distributed and concentrated. While nonlinear behaviors such as free play, hysteresis and friction are examples of concentrated nonlinear features, material non-linearity and deformation non-linearity are examples of distributed nonlinear features.

In nonlinear systems, most of the problems do not have exact solution, so that iterative methods are used. In solution of nonlinear aeroelastic problems, implicit or explicit Euler's time integration methods are highly used. Another solution method that is valid for the systems which have periodic response is harmonic balance method. Runge-Kutta method also gives very close results to exact ones. It should not be forgotten that all of these methods depends on the initial conditions and time step size, getting convergence in highly nonlinear system could be very challenging task.

The free-play is firstly studied by Woolston et al [23]. In this study, it is stated that the LCO may arise before linear flutter speed. Yang and Zhao investigated the effects of asymmetric freeplay effects on the stability of a typical section using harmonic balance method [24]. In this work, the divergent behavior observed at the linear flutter speed and LCOs was seen before linear boundary. McIntosh et al. studied the effects of hardening and softening stiffness effect on the stability of a typical section [25]. They founded that the dynamical behavior of the typical section can be summarized as; the LCOs may emerge with a fixed amplitude fixed frequency, may or may not show LCO behavior depends on the initial condition. In the context of nonlinear dynamics these behavior can be called as subcritical and supercritical behavior. More recent study on the effects of structural nonlinearities on a typical section was studied Chung et al [26]. They use perturbation incremental method for the study of limit cycles and bifurcations of the typical system. The implementation of the perturbation incremental method provided to model the system with C^0 continuous stiffness such as bilinear stiffness or freeplay. The founded results were in good agreement with literature that shows the subcritical behavior. Another highly referred

work belongs to Conner et al. [27]. In Conner's and his friends work, the effects of free-play are investigated both mathematically and experimentally. The geometrical, structural and inertial properties which used in the present study are taken from Conner's to validate the model. Saied et al investigates the effects of the order of harmonic balance at 3-DOF typical section with cubic stiffness nonlinearity. [28] They founded that, in some case harmonic balance of order one was not sufficient to capture flap amplitudes accurately.

The nonlinear analyses in 3D domain require more tedious work. The fictitious mass (FM) method [29] is one of the popular methods that used in reducing the size of the problem and solution time. In the FM method, a large mass is added to DOF where the sudden change occurs. In addition to that, generalized coordinates are able to represent nonlinear changes with FM added generalized coordinates. The solution process of the FM is similar to the normal mode analysis with added fictitious mass in the mass matrix. Lee and Chen applied FM method on a folding wing with free-play hinge nonlinearity using ZAERO and MSC.Nastran [30]. They investigated the effects of varying free-play angle for various folding angles. They founded that LCO can still be present event the higher altitudes then the altitudes flutter observed due to free-play.

The component mode synthesis method (CMS) is using modal coupling method to model complex structure by dividing into components and solve separately and synthesis of the results to achieve the solution of whole structure. In this method, the interface at the region of divided component and main structure is modeling coupling either displacement or forces. Ning et al. present a new modeling method using CMS to model free-play nonlinearity [4]. They studied a folding-fin structure with various free-play angles. They performed numerical analyses and wind tunnel experiments. They founded that the increasing free-play angle provide higher divergent speed. The most important outcome of the study that states the linear flutter analysis results are conservative and provide safe flight conditions.

The studies on the effects of structural nonlinearities on more complex structures are still an ascending area of interest among many aeroelasticians. The Fighting Falcon F-16 aircrafts is one of the mostly studied aircraft owing to its LCO prone characteristic. The limitations of the linear structural and aerodynamic approaches cause to miss the LCO behavior of the aircraft. At the speed where LCO arise can be different from the flutter speed. For this reason, the amplitude and the airspeed of the LCO are important parameters for flight safety. Some of the researchers thought that the LCO mechanism in F-16 is a conclusion of oscillation of transonic aerodynamic shocks and another group of researcher the bounding mechanism of LCO is created due to structural effects. Zhang et al. [31] investigate the results of the first group which relate LCO with nonlinear aerodynamics and stated that the sole nonlinear aerodynamics does not explain the LCO as the aircraft shows LCO behaviors at the airspeed 0.6 and 1.4 Mach. As these speeds are not in the transonic range and there would be no transonic shock on the aircraft wing. According to these informations, the nonlinear aerodynamics cannot be only reason for LCO to arise. Fearnow [32] investigates the damping change for increasing amplitude of oscillations. He found that the damping of the system increases with increasing amplitudes. Dossogne et al. [33] shows that the changing damping mechanism of the full-scale F-16 using sine-sweep tests. For this reason implementing this nonlinearity provides better physical representation for aeroelastic analysis. In this manner, ZONA Technology developed a nonlinear modeling method that provides nonlinear damping implementation. This method depends on assumption of any mechanical joint provide stabilizing effect with the help of dry friction. The flight test results are compared to results from nonlinear module of ZEUS which uses Euler aerodynamics and seen good agreement for this specific store configuration. The results are given in the Figure 1.11.
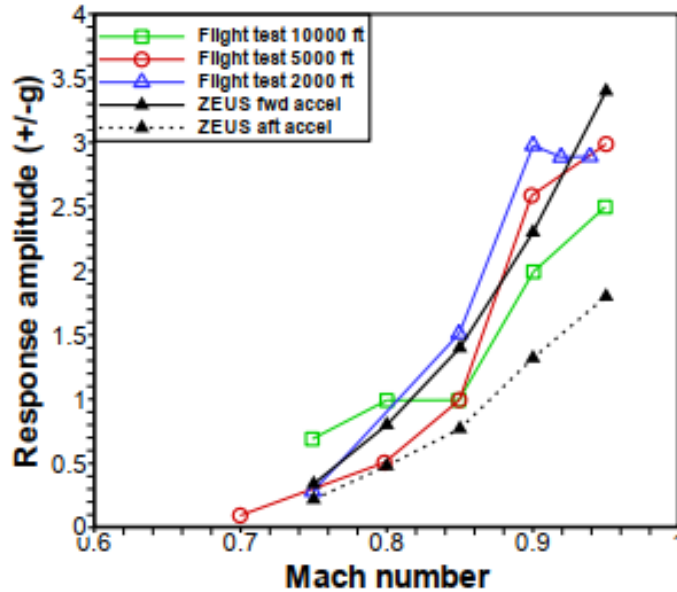
Figure 1.11. Comparison of LCO amplitudes from test and nonlinear ZEUS analysis

All air vehicles must be certified in a manner of airworthiness along the flight envelope that guarantees the stability of the vehicle. The certification of aircrafts for a new store is the mostly studied aeroelastic phenomenon in TÜBİTAK SAGE. The certification of the aircraft for new stores is conducted according to MIL-HDBK-1763. The certification steps are modal analysis, pre-aeroelastic analysis ground vibration test, modal updating, aeroelastic analysis for updated model and flight test. Some of the academic contributions are briefly explained in following lines. The flutter characteristics of plate like structures investigated through ZAERO and wind tunnel test [34]. In this study, flutter solution methods such as k-method and g-method of ZAERO is compared. The g-method results are found as more reliable for rectangular plate and F-16 wing shaped plate with a store on the wing tip. In another work, flutter analysis and simulated flutter test of wings is studied. In this study, flutter speed is calculated for a linear 2D typical section and comparison performed from NASTRAN Flight Loads software. In this study, flutter speed estimation models are also studied [35]. Apart from this work, aeroelastic stability determination using flight test datas is studied and reliable prediction methods are compared and a new method is presented [36]. In a recent study, effects of design parameters such as taper ratio, aspect ratio and sweep angle on the aeroelastic stability of a cruise missile wing is studied [37] . It

is found that, the increment on the aspect ratio and taper ratio causes lower flutter speed. On the other hand, the sweep angle provides higher flutter speed in general.

In this section, the enhancements and the new methodologies for linear and nonlinear aeroelasticity are examined. The articles and theses from both industrial and academic areas are studied.

2. AEROELASTIC MODELING OF 3 DOF TYPICAL SECTION

In this section the aeroelastic modeling of a 3 DOF wing-aileron section is obtained. In the first part the equation of motion for the structural model is obtained. In the second part the aerodynamic modeling will be explained. Finally, in the third part, the aeroelastic equation of motion will be derived using structural and aerodynamic model.

2.1. Structural Modeling of 3 DOF Typical Section

As mentioned in the earlier sections, the typical section which has two degree of freedoms is widely used for aeroelastic response calculations. This approach gives meaningful results generally for infinite non-tapered and unswept wings. As it mentioned before, the motivation behind this work is becoming familiar with nonlinear aeroelasticity. So that, working on a 2D typical section would be a good starting point.

The typical section with the ability to move in pitch, plunge and aileron rotation direction is given in Figure 2.1. The distance x_f defines the position of elastic axis, x_h defines the position of aileron hinge, c is the chord length and finally b is the half – chord length. The displacement in vertical direction is denoted by h, the rotation about x_f is denoted by α and finally the rotation about x_h is denoted by β.
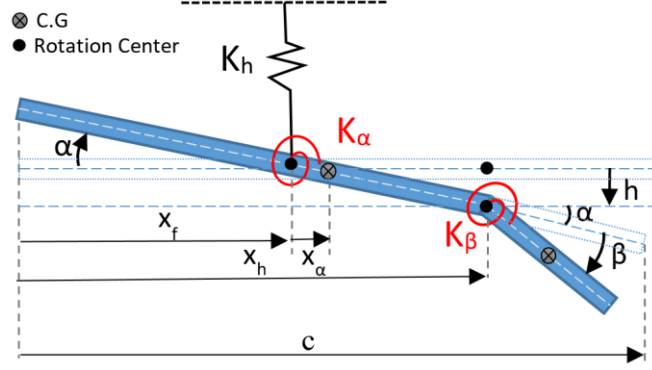
Figure 2.1. 2D Typical Section with 3 DOFs

The positive directions are downward in the plunge direction, clockwise rotation in the pitch and control section directions. m is the mass per unit length, S_α is the static mass moment around x_f and I_α is the mass moment of inertia around x_f. S_β is the static mass moment around x_h, I_β is the mass moment inertia around x_h and finally $I_{\alpha\beta}$ is defined as the summation of I_β with the static mass moment S_β times the distance between control surface hinge and elastic axis that emerges due to coupled motion of airfoil and control surface. The force vector includes aerodynamic lift, aerodynamic moment around x_f and aerodynamic moment around x_h. The stiffness and damping terms are denoted as K_j and C_j where $j = \{h, \alpha, \beta\}$. The equation of motion of the system is obtained via Lagrange method. The Lagrangian of a system can be defined as

$$L = T - V \qquad\qquad 2.1$$

where T and V denote kinetic and potential energy of the system. The application of the virtual displacement method on a non-conservative system can be shown as in Equation 2.2.

$$\frac{d}{dt}\left(\frac{\partial L}{\partial \dot{x}_i}\right) - \frac{\partial L}{\partial x_i} + \frac{\partial D}{\partial \dot{x}_j} = Q \qquad j = \{h, \alpha, \beta\} \qquad\qquad 2.2$$

D and Q denote dissipative terms and external forces. The kinetic and potential energies of the system and the dissipated energy from the system are given as follows. The external forces are aerodynamic lift and moments which will be given in the Section 2.2.

18

$$T = \frac{1}{2}m(\dot{h})^2 + \frac{1}{2}I_\alpha(\dot{\alpha})^2 + \frac{1}{2}I_\beta(\dot{\beta})^2 + \frac{1}{2}S_\beta\dot{h}\dot{\beta} + \frac{1}{2}S_\alpha\dot{h}\dot{\alpha} + \frac{1}{2}I_{\alpha\beta}\dot{\alpha}\dot{\beta} \qquad 2.3$$

$$V = \frac{1}{2}K_h(h)^2 + \frac{1}{2}K_\alpha(\alpha)^2 + \frac{1}{2}K_\beta(\beta)^2 \qquad 2.4$$

$$D = \frac{1}{2}C_h(\dot{h})^2 + \frac{1}{2}C_\alpha(\dot{\alpha})^2 + \frac{1}{2}C_\beta(\dot{\beta})^2 \qquad 2.5$$

The Lagrangian of the system can be obtained substituting Equations 2.3 and 2.4 in to 2.1.

$$\begin{aligned} L = &\frac{1}{2}m(\dot{h})^2 + \frac{1}{2}I_\alpha(\dot{\alpha})^2 + \frac{1}{2}I_\beta(\dot{\beta})^2 + \frac{1}{2}S_\beta\dot{h}\dot{\beta} + \frac{1}{2}S_\alpha\dot{h}\dot{\alpha} + \frac{1}{2}I_{\alpha\beta}\dot{\alpha}\dot{\beta} \\ &-\frac{1}{2}K_h(h)^2 - \frac{1}{2}K_\alpha(\alpha)^2 - \frac{1}{2}K_\beta(\beta)^2 \end{aligned} \qquad 2.6$$

It is possible to see the damping and stiffness terms are uncoupled. Substituting Equation 2.5 and 2.6 into 2.2 will give the final form.

$$\begin{aligned} &m\ddot{h} + I_\alpha\ddot{\alpha} + I_\beta\ddot{\beta} + S_\alpha\ddot{\alpha} + S_\beta\ddot{\beta} + S_\alpha\ddot{h} + S_\beta\ddot{h} + I_{\alpha\beta}\ddot{\beta} + I_{\alpha\beta}\ddot{\alpha} + K_h h + K_\alpha\alpha \\ &+ K_\beta\beta + C_h\dot{h} + C_\alpha\dot{\alpha} + C_\beta\dot{\beta} \end{aligned} \qquad 2.7$$

The above equation can also be written in matrix form as given below.

$$\begin{bmatrix} m & S & S_\beta \\ S & I_\alpha & I_{\alpha\beta} \\ S_\beta & I_{\alpha\beta} & I_\beta \end{bmatrix}\begin{bmatrix} \ddot{h} \\ \ddot{\alpha} \\ \ddot{\beta} \end{bmatrix} + \begin{bmatrix} C_h & 0 & 0 \\ 0 & C_\alpha & 0 \\ 0 & 0 & C_\beta \end{bmatrix}\begin{bmatrix} \dot{h} \\ \dot{\alpha} \\ \dot{\beta} \end{bmatrix} + \begin{bmatrix} K_h & 0 & 0 \\ 0 & K_\alpha & 0 \\ 0 & 0 & K_\beta \end{bmatrix}\begin{bmatrix} h \\ \alpha \\ \beta \end{bmatrix} = \begin{pmatrix} -L \\ M_\alpha \\ M_\beta \end{pmatrix} \qquad 2.8$$

The force vector added to right side of the equality which will be obtained from the aerodynamic lift and moments.

2.2. Aerodynamic Modeling of 3 DOF Typical Section

In this thesis, simplified airfoil geometry with a control section will be investigated which is generally called as typical section. Although a typical section analysis is a simplified model and valid for only certain conditions it could give very important and powerful insights. Application of the potential theory in typical section does not require tedious work and it is frequently used to estimate the 3D wing behavior in both academic and industrial works.

The 3DOF typical section was given in Figure 2.1 and the equation of motion of the wing-aileron system was given in 2.8. The force vector includes aerodynamic lift, aerodynamic moment around elastic axis and aerodynamic moment around control surface rotation axis. The force vector can also be written in the form of aerodynamic mass, stiffness and damping.

In potential flow, conformal mapping is used for modeling flow around an airfoil by using flow around a circle. It is need to satisfy Kutta condition to apply this method. The Kutta condition states that there is no flow on the trailing part of the airfoil which also means that the rear stagnation point is relocated at the trailing edge.
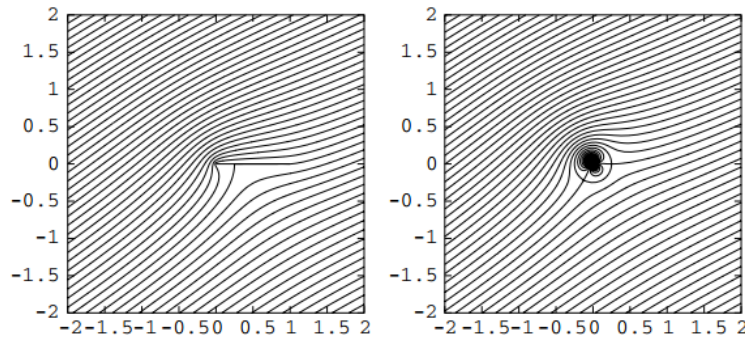
Figure 2.2. Conformal mapping of a circle and flat plate [38]

Theodorsen applied this method to oscillating wing or airfoil [21]. In his work, the wing-aileron system in 2D is studied. This work is apart from the studies of Theodorsen with introducing nonlinear elements on different degree of freedoms and solution methods. This part of the thesis is referenced from the work of Theodorsen.

The geometry of the typical section with a control surface (aileron) has an importance for aerodynamic forces such as; the location of center of gravity, aileron hinge location, the distance between center of gravity and center of elasticity etc. The typical section with a control surface representation is given Figure 2.3 once more. The dimensionless values a and c_h which reduced according to the semi-chord length b, can be defined as below and the variable μ is defined which equals $\cos^{-1} c_h$.
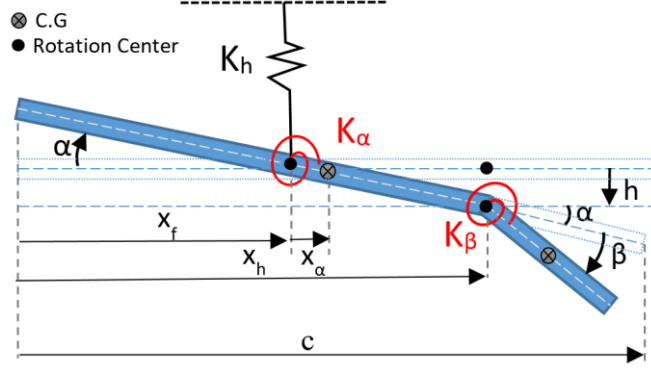
Figure 2.3. 2D Typical Section with 3 DOFs

$$a = \frac{x_f}{b} - 1 \qquad\qquad 2.9$$

$$c_h = \frac{x_h}{b} - 1 \qquad\qquad 2.10$$

The force and moments that are calculated using potential flow theory are given in the equations between 2.11 and 2.13. The force and moments equations were obtained in frequency domain.

$$L = -\rho b^2 \left[U\pi\dot{\alpha} + \pi\ddot{h} - \pi ba\ddot{\alpha} - UT_4\dot{\beta} - T_1 b\ddot{\beta} \right]$$
$$- 2\pi\rho UbC(k)\left[U\alpha + \dot{h} + b\left(\frac{1}{2} - a\right)\dot{\alpha} + \frac{T_{11}}{\pi}U\beta + b\frac{T_{11}}{2\pi}\dot{\beta} \right] \qquad 2.11$$

$$M_{x_h} = -\rho b^2 \left[\left(-2T_9 + T_1 + T_4\left(a - \frac{1}{2}\right) \right) bU\dot{\alpha} + 2T_{13}b^2\ddot{\alpha} \right.$$
$$+ \frac{1}{\pi}U^2\beta(T_5 - T_4 T_{10}) - \frac{1}{2\pi}Ub\dot{\beta}T_4 T_{11} - \frac{1}{\pi}T_3 b^2\ddot{\beta} - T_1 b\ddot{h} $$
$$\left. - \rho Ub^2 C(k)T_{12}\left[U\alpha + \dot{h} + b\left(\frac{1}{2} - a\right)\dot{\alpha} + \frac{T_{11}}{\pi}U\beta + b\frac{T_{11}}{2\pi}\dot{\beta} \right] \right. \qquad 2.12$$

$$M_{x_f} = -\rho b^2 \left[\pi \left(\frac{1}{2} - a \right) U b \dot{\alpha} + \pi b^2 \left(\frac{1}{8} + a^2 \right) \ddot{\alpha} + (T_4 + T_{10}) U^2 \beta \right.$$
$$+ \left(T_1 - T_8 - (c_h - a) T_4 + \frac{1}{2} T_{11} \right) U b \dot{\beta} - (T_{7+}(c_h - a) T_1) b^2 \ddot{\beta}$$
$$\left. - a \pi b \ddot{h} \right] \qquad\qquad 2.13$$
$$- 2 \rho U b^2 C(k) \pi \left(a + \frac{1}{2} \right) \left[U \alpha + \dot{h} + b \left(\frac{1}{2} - a \right) \dot{\alpha} + \frac{T_{11}}{\pi} U \beta \right.$$
$$\left. + b \frac{T_{11}}{2\pi} \dot{\beta} \right]$$

The Theodorsen function has real and imaginary parts such as $C(k) = F(k) + iG(k)$ where the parameter k is defined as reduced frequency. The $F(k)$ and $G(k)$ are the first and second kind of Bessel functions. T_j, $j = \{1 \dots 16\}$ are aerodynamic constants which are given in the following lines.

$$T_1 = -\frac{1}{3} \sqrt{1 - c_h^2} (2 + c_h^2) + c_h \mu$$

$$T_2 = c_h (1 - c_h^2) - \sqrt{1 - c_h^2} (1 + c_h^2) \mu + c_h \mu^2$$

$$T_3 = -\left(\frac{1}{8} + c_h^2 \right) \mu^2 + \frac{1}{4} c_h \sqrt{1 - c_h^2} \mu (7 + 2c_h^2) - \frac{1}{8} (1 - c_h^2)(5c_h^2 + 4)$$

$$T_4 = -\mu + c_h \sqrt{1 - c_h^2}$$

$$T_5 = -(1 - c_h^2) - \mu + 2c_h \sqrt{1 - c_h^2} \mu$$

$$T_6 = T_2$$

$$T_7 = -\left(\frac{1}{8} + c_h^2 \right) \mu + \frac{1}{8} c_h \sqrt{1 - c_h^2} (7 + 2c_h^2)$$

$$T_8 = -\frac{1}{3} \sqrt{1 - c_h^2} (2c_h^2 + 1) + c_h \mu$$

$$T_9 = \frac{1}{2} \left[\frac{1}{3} \sqrt{1 - c_h^2} + aT_4 \right]$$

$$T_{10} = \sqrt{1 - c_h^2} + \mu$$

$$T_{11} = \mu (1 - 2c_h) + \sqrt{1 - c_h^2} (2 - c_h)$$

$$T_{12} = \sqrt{1 - c_h^2}(2 + c_h) - \mu(2c_h + 1)$$

$$T_{13} = \frac{1}{2}(-T_7 - (c_h - a)T_1)$$

$$T_{14} = \frac{1}{16} + \frac{1}{2}ac_h$$

The abovementioned force and moments can be transferred into the time domain using Fourier Transform which is performed by Wagner and the new function is called with his name. The Wagner function Φ is used for unsteady modeling of aerodynamics. The difference between Theodorsen and Wagner's method is the domain of solution. These two methods can be transformed one to another by using Fourier and inverse Fourier transforms. The Wagner function is defined in Eq.2.14 that creates the effect of unsteady aerodynamic on lift which can be seen in Figure 2.4.

$$\Phi(t) = 1 - \Psi_1 e^{-\frac{\varepsilon_1 Ut}{b}} - \Psi_2 e^{-\varepsilon_2 Ut/b} \qquad 2.14$$
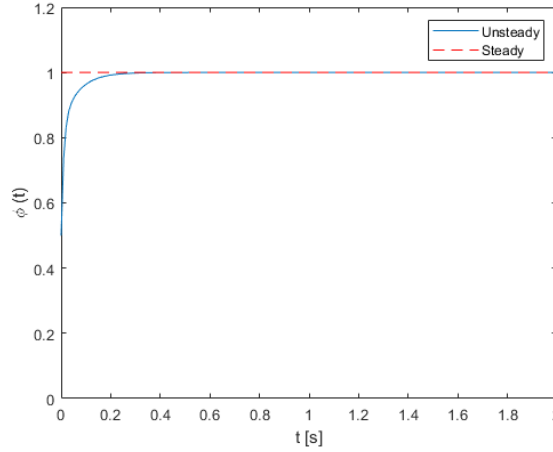
Figure 2.4. Unsteady and Steady Lift vs. time

The transformation between Theodorsen and Wagner functions can be defined as follows.

$$C(k)w = \Phi(0)w - \int_0^t \frac{\partial \Phi(t - t_0)}{\partial t_0} w(t_0)dt_0 \qquad 2.15$$

The force and moments equations are rewritten in time domain using above transformation.

$$L(t) = \rho b^2 \left(U\pi\dot{\alpha} + \pi\ddot{h} - \pi b a\ddot{\alpha} - UT_4\dot{\beta} - T_1 b\ddot{\beta}\right)$$
$$+ 2\pi\rho bU\left(\Phi(0)w - \int_0^t \frac{\partial\Phi(t-t_0)}{\partial t_0}w(t_0)dt_0\right) \qquad 2.16$$

$$M_{x_h}(t) = -\rho b^2 \left(-T_1 b\ddot{h} + 2T_{13}b^2\ddot{\alpha} - \frac{1}{\pi}T_3 b^2\ddot{\beta}\right)$$
$$- \rho b^2 \left(\left(-2T_9 - T_1 + T_4\left(a - \frac{1}{2}\right)\right)Ub\dot{\alpha} - \frac{1}{2\pi}UbT_4T_{11}\dot{\beta}\right)$$
$$- \frac{\rho b^2 U^2}{\pi}(T_5 - T_4T_{10})\beta \qquad 2.17$$
$$- \rho b^2 UT_{12}\left(\Phi(0)w - \int_0^t \frac{\partial\Phi(t-t_0)}{\partial t_0}w(t_0)dt_0\right)$$

$$M_{x_f}(t) = -\rho b^2 \left(-a\pi b\dot{h} + \pi b^2\left(\frac{1}{8} + a^2\right)\ddot{\alpha} - T_7 + (c_h - a)T_1\right)b^2\ddot{\beta}$$
$$- \rho b^2 \left(\pi\left(\frac{1}{2} - a\right)Ub\dot{\alpha} + \left(T_1 - T_8 - (c_h - a)T_4 + \frac{T_{11}}{2}\right)Ub\dot{\beta}\right) \qquad 2.18$$
$$- \rho b^2 (T_4 + T_{10})U^2\beta$$
$$+ 2\rho Ub^2\pi\left(a + \frac{1}{2}\right)\left(\Phi(0)w - \int_0^t \frac{\partial\Phi(t-t_0)}{\partial t_0}w(t_0)dt_0\right)$$

The terms that consists integration of Wagner function in lift and moment equations can be solved as follows.

$$\Phi(0)w - \int_0^t \frac{\partial\Phi(t-t_0)}{\partial t_0}w(t_0)dt_0$$
$$= \Phi(0)w(t) - \left(h(0) + b\left(\frac{1}{2} - a\right)\alpha(0) + b\frac{T_{11}}{2\pi}\beta(0)\right)\dot{\Phi}(t)$$
$$+ \left(h(t) + b\left(\frac{1}{2} - a\right)\alpha(t) + b\frac{T_{11}}{2\pi}\beta(t)\right)\dot{\Phi}(0)$$
$$- \Psi_1\left(\frac{\varepsilon_1 U}{b}\right)^2 w_1(t) - \Psi_2\left(\frac{\varepsilon_2 U}{b}\right)^2 w_2(t)$$
$$+ \Psi_1\frac{\varepsilon_1 U^2}{b}\left(1 - \varepsilon_1\left(\frac{1}{2} - a\right)\right)w_3(t) \qquad 2.19$$
$$+ \Psi_2\frac{\varepsilon_2 U^2}{b}\left(1 - \varepsilon_2\left(\frac{1}{2} - a\right)\right)w_4(t)$$
$$+ \Psi_1\frac{\varepsilon_1 U^2}{b\pi}\left(T_{10} - \frac{\varepsilon_1 T_{11}}{2}\right)w_5(t)$$
$$+ \Psi_2\frac{\varepsilon_2 U^2}{b\pi}\left(T_{10} - \frac{\varepsilon_2 T_{11}}{2}\right)w_6(t)$$

where $\Psi_1 = 0.165$, $\Psi_2 = 0.335$, $\varepsilon_1 = 0.0455$, $\varepsilon_2 = 0.3$ and w_i, $i = 1 \dots 6$ are the aerodynamic states.

2.3.   Aeroelastic Equation of Motion

The given aerodynamic force and moment equations can be manipulated to acquire acceleration, velocity and displacement terms for plunge, pitch and control surface degree of freedoms. The coefficient of acceleration, velocity and displacement terms are called aerodynamic mass, aerodynamic damping and aerodynamic stiffness. These coefficients make contribution to structural behavior. The aeroelastic equation of airfoil with a control section is obtained by manipulating the acceleration, velocity and displacement terms in both structural and aerodynamic equations. The matrix form of the aeroelastic equation is given as below.

$$(A + \rho B)\ddot{x} + (C + \rho U D)\dot{x} + (E + \rho U^2 F)x + \rho U^3 Ww = \rho U g \Phi(t)$$
$$\dot{w} - W_1 x - U W_2 w = 0$$

2.20

The term $\rho U g \Phi(t)$ states external excitation and its effects can be neglected since these effects decay in a short time. The aeroelastic equation of motion (AEOM) of a typical section with 3 DOFs can be transformed into matrix form such as given in 2.21

$$Q = \begin{bmatrix} -(A + \rho B)^{-1}(C + \rho U D) & -(A + \rho B)^{-1}(E + \rho U^2 F) & -(A + \rho B)^{-1}(\rho U^3 W) \\ I_{3 \times 3} & 0_{3 \times 3} & 0_{6 \times 3} \\ 0_{6 \times 3} & W_1 & U W_2 \end{bmatrix}$$

2.21

$$x = \begin{bmatrix} \dot{h} & \dot{\alpha} & \dot{\beta} & h & \alpha & \beta & w_1 & w_2 & w_3 & w_4 & w_5 & w_6 \end{bmatrix}^T$$

2.22

$$\dot{x} = Qx$$

2.23

where **A, C, E** are structural mass, damping and stiffness matrices and **B, D, F** are aerodynamic mass, damping and stiffness matrices. **W** is aerodynamic influence matrix and W_1 and W_2 aerodynamic state matrix. h, α and β are displacements in plunge, pitch and control surface directions. Finally, w_i, $i = 1 \dots 6$ are aerodynamic states. Each structural and aerodynamic matrix will be given explicitly in the appendix.

25

3. LINEAR AND NONLINEAR SOLUTION APPROACHES

In this section the solution approaches and the foundation of the numerical analysis will be explained. At first, the solution of linear model with eigenvalue solution in the time domain will be explained. Secondly, solution of linearized version of a nonlinear model will be explained. And finally, the nonlinear theory, solution techniques and the information about the software package MATCONT will be given.

3.1. Eigenvalue Solution

The stability of the linear aeroelastic equation of motion can be defined by eigenvalue problem. The solution of above AEOM will give the stability of the linear system. The results of the eigenvalue problem can be manipulated into frequency, damping and the mode shapes that change with airspeed. An eigenvalue problem can be shown as follows

$$\dot{x} - Qx = 0 \qquad\qquad 3.1$$

The eigenvalues of the matrix Q can be found as shown below,

$$|I\lambda - Q| = 0 \qquad\qquad 3.2$$

Equation 3.2 is generally called as characteristic equation. The roots of the equation are eigenvalues. The aeroelastic flutter is the case where the total damping of the system is less than zero. Another indication of flutter, the frequencies of two modes shape getting closer or becoming identical. The AEOM is obtained using Wagner approach for unsteady aerodynamic modeling and Lagrange method. The solutions for damping and frequency are obtained using following equations where i stands for number of states.

$$\omega_i = |\lambda_i| \quad i = \{1,2,3\} \qquad\qquad 3.3$$

$$\zeta_i = -\frac{Re(\lambda_i)}{\omega_i} \quad i = \{1,2,3\} \qquad\qquad 3.4$$

3.2.   Nonlinear Modeling and Solution Techniques

The solution of the aeroelastic equation of motion that given in 2.20 can be solved with time integration methods. However, time integration method is inefficient while acquiring solution at higher airspeed. Also, the characteristic of the nonlinear system could not be fully understood with time integration methods. The stability, bifurcations, LCO behavior of the system should be obtained to understand dynamics of the nonlinear system. The nonlinear bifurcation analysis and time response results are obtained with an open-source package software, MATCONT. MATCONT [39], is a MATLAB package for solving continuous and discretized systems for stability analysis, bifurcation analysis, calculation and classification of branch points and system response calculation for multiple parameters. MATCONT uses numerical continuation method with discretization methods for solving ODEs. The capabilities, theory behind and usage of MATCONT are briefly explained in following paragraphs.

3.2.1   Numerical Continuation

The nonlinear systems can have many solutions and may not have general solution. The famous Newton – Raphson method can be inadequate and cannot find all the solutions for the interested regions. For example, if a single DOF mechanical system has a cubic stiffness, the frequency response of the system for an excitation will follow a path according to the sign of the stiffness. The positive stiffness causes hardening and negative stiffness causes softening behaviors. The solution of these systems is not possible while using Newton – Raphson method if the system is highly nonlinear. The Harmonic Balance (HB) method results of well-known Duffing Oscillator are presented in Figure 3.1. The Fourier coefficients of HB method are calculated with using Newton – Raphson method. It can be seen that as the nonlinearity increases, there is a sudden drop on the curves.
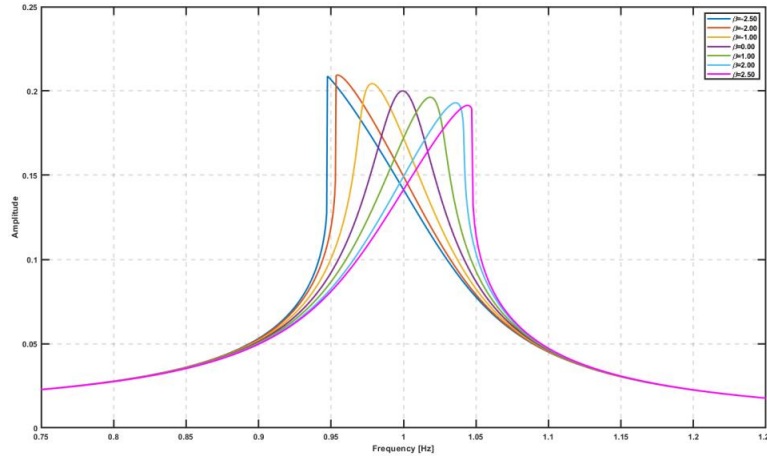
Figure 3.1. Duffing Oscillator Newton Raphson Method Results

The Newton - Raphson method become inefficient in the case of if the initial guess is not good enough and if the solution has multiple branches such as hardening and softening behavior on mechanical systems. In these cases, parameterization of one of the system properties may enhance the solution. The numerical continuation methods provide more robust solutions. The numerical continuation equality can be represented simply as in 3.5.

$$f(x, \lambda) = 0 \qquad\qquad 3.5$$

where f is a $n \times 1$ vector and λ is one of the system parameter. The free parameter can be frequency, cubic stiffness or quadratic damping constant. One of the drawbacks of the numerical continuation is, it is not possible to force Newton predictor to find the all the solution in the desired branch. But it is possible to manipulate Newton predictor using prediction correction. For a visual understanding of the mentioned methods Duffing oscillator is also studied with numerical continuation. The frequency response of the previous Duffing oscillator is calculated with numerical continuation method and given in Figure 3.2. If the system is weakly nonlinear it is possible to obtain same solution with both numerical continuation and Newton – Raphson method.
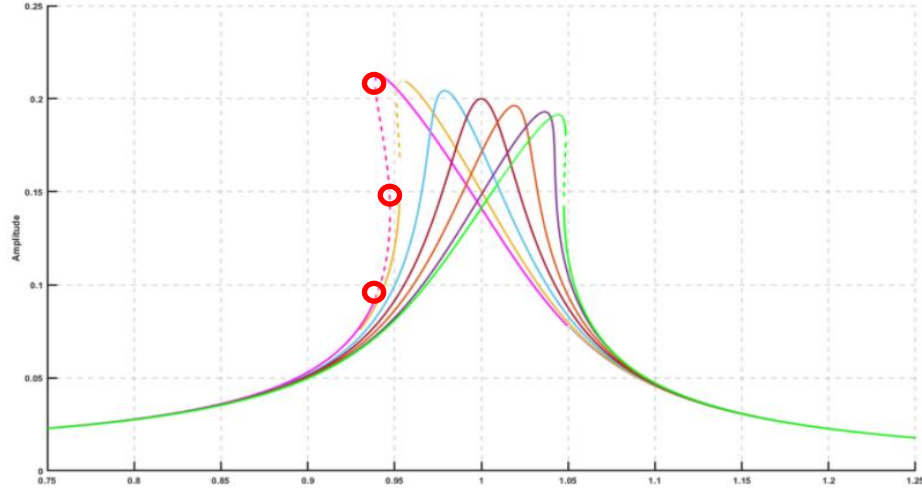
Figure 3.2. Duffing Oscillator Numerical Continuation Method

In Figure 3.2 the marked circles show that a new prediction correction vector is needed and these vectors must be introduced manually. The first guess for the vector should be good enough otherwise the method would not converge. It is possible to handle these disadvantages by using arclength continuation. The arclength continuation method can follow the path at turning point where multiple solutions are present. The method is based on the idea of using arclength parameter s instead of the natural parameter λ which is also a function of s. The arclength parameter s is the radius of a sphere where the solution of the system is sought. After the first prediction near the turning point, the algorithm searches for solutions within the sphere according to a defined error criterion. The value of s is important to find correct solution. If s value is larger than it should be, the algorithm may find another solution which disrupts the continuity of the path.

The pseudo-arclength method is based on arclength continuation method to improve solution process. In arclength continuation method the continuation may go back since two or more points satisfy the arclength equation. The pseudo arclength method provides a solution that prevents continuation to reverse its direction. The method uses prediction vector as a solution method. The solution is sought in the perpendicular direction of prediction vector. The representations of pseudo – arclength and arclength continuation methods are given in Figure 3.3. On the other hand, MATCONT uses a version of Moore-

Penrose continuation which is also a variant of pseudo – arclength continuation method and its representation is given in Figure 3.4. MATCONT uses equilibria and limit cycles continuation for ordinary differential equations for obtaining bifurcation points.
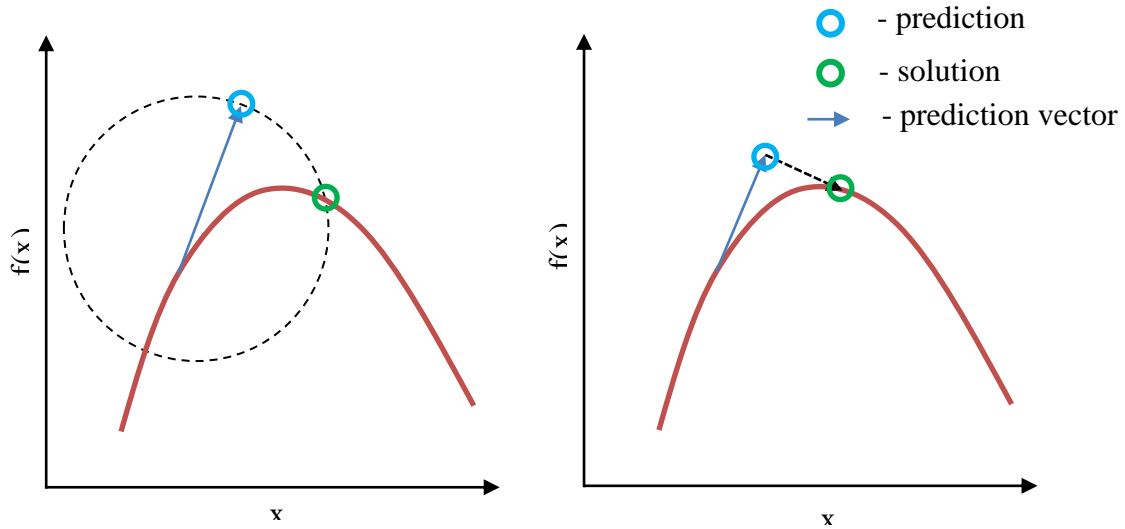
Figure 3.3. The representation of arclength and pseudo-arclength continuation
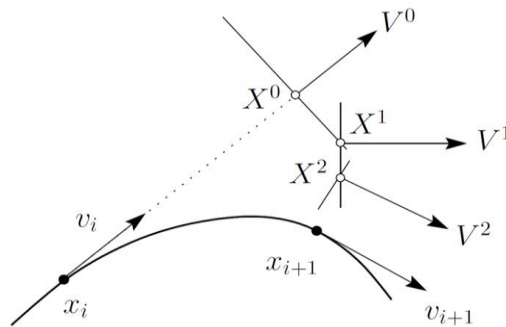
Figure 3.4. The representation of Moore-Penrose continuation method

3.2.2   Bifurcation Analysis

In nonlinear dynamics, the bifurcation theory shows the effects of varying system parameters on the system. Bifurcation point can be defined as where there is a change in the stability or equilibrium (fixed) point behavior of the nonlinear dynamical system. The nonlinearity sources are chosen as cubic stiffness, quadratic damping and free-play in this

thesis. The typical section model with nonlinearities is studied to understand the effects of nonlinear sources on an aeroelastic system. The types of bifurcation depend on eigenvalues of the system and indicate different types of dynamics. A brief explanation of the types of bifurcation is presented in following paragraphs.

3.2.2.1. Hopf Bifurcation

The Hopf bifurcation occurs when both of the complex conjugate eigenvalues cross the positive part of the phase plane as the parameter λ changes in Eq. 3.5. The parameter λ reaches critical value at λ_c where the responses do not damp out anymore. The representation of the Hopf bifurcation is given in Figure 3.5. As can be seen in this figure, at the Hopf point the oscillations start and increase with the parameter. So that, the Hopf bifurcation can be explained as bifurcation from equilibria to oscillation.

The Hopf bifurcation is classified into supercritical and subcritical Hopf bifurcation. As the parameter λ is getting closer to the critical value, the rate of damping is also getting closer to zero. Eventually, at the critical value of damping, the system shows periodic and constant amplitude sinusoidal response. The amplitude of the response depends on also the λ parameter. For the subcritical Hopf bifurcation, after λ value reaches the critical value the system become unstable and the response can go to another orbit, limit cycle or infinity. As oppose the supercritical Hopf bifurcation, subcritical Hopf bifurcation is more dangerous in engineering.
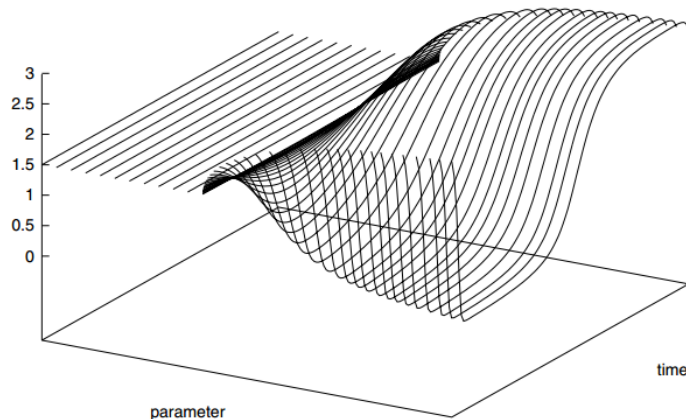
Figure 3.5. Bifurcation from equilibria to oscillations [40].

31

3.2.2.2. Fold Bifurcation

The destruction or creation of fixed points is called fold or saddle-node bifurcation. One of the new fixed points is stable and the other one is unstable and as the parameter increases the fixed points getting away from each other. At the fold bifurcation the derivative of the LCO amplitude with respect to parameter become infinite. Being derivative is infinite, the sign of the derivative changes sign. It means that the fold bifurcation occurs at turning points. At the fold point LCO is half stable. The illustration of the fold bifurcation is given in Figure 3.6.
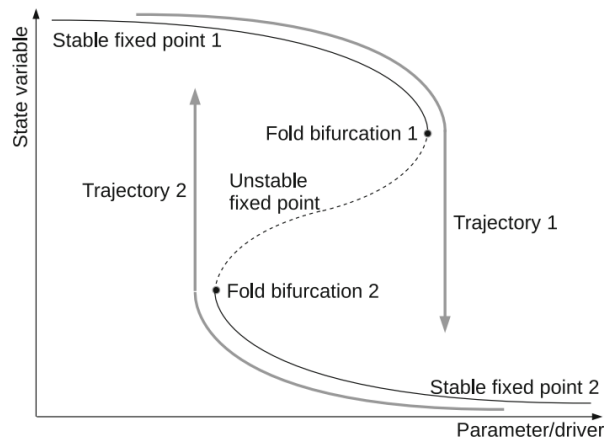
Figure 3.6. Illustration of fold bifurcation on a bifurcation diagram

3.2.2.3. Neimark-Sacker Bifurcation

The Neimark-Sacker (NS) bifurcation can be explained as Hopf bifurcation of LCO. The NS bifurcation is also called as torus bifurcation as well. The NS bifurcation happens when a pair of complex eigenvalues has unity in modulus. In the presence of NS, the characteristics of LCO changes from pure sinusoidal to aperiodicity. The NS bifurcation is also divided into as subcritical and supercritical. The supercritical NS bifurcation transforms stable limit cycle to unstable limit cycle and a stable torus born. The subcritical NS bifurcation transforms stable limit cycle to unstable limit cycle and unstable torus.

For the aeroelastic point of view, to NS bifurcation occurs there must be more than one flutter mechanism which is triggered with the fundamental LCO frequency. The

transformation from limit cycle to NS can be explained via using phase planes that given in Figure 3.7.
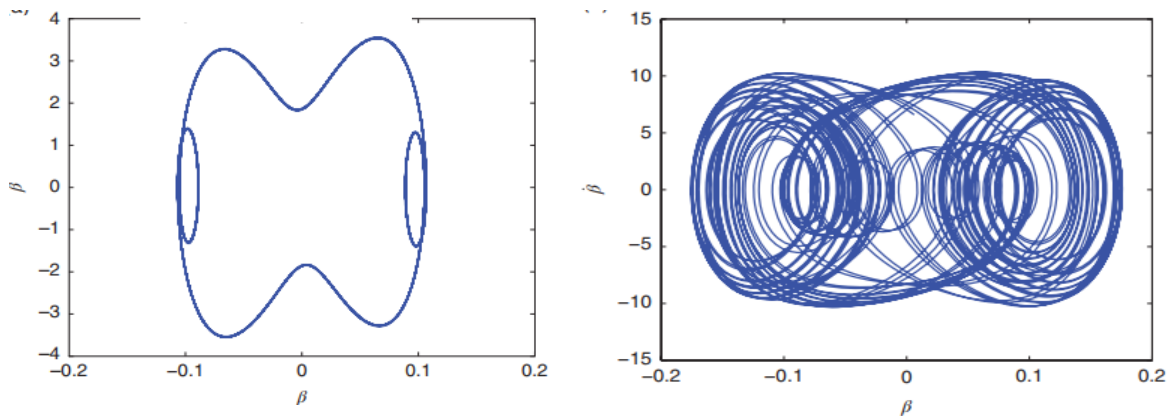
Figure 3.7. NS bifurcation- LCO to Torus [41]

3.2.2.4. Period Doubling

The periodic doubling is a phenomenon that caused when a slight change in system parameter which causes to born a new trajectory. The period of this new trajectory has the period where the period doubled compared to the previous one. The periodic doubling bifurcation is more chaotic phenomenon than Hopf bifurcation and occurs on the limit cycle curve which is born due to Hopf bifurcation. The periodic doubling bifurcation has also subcritical and supercritical definition that transforms stable orbits to unstable orbits with doubling the period or vice versa. The phase plane of a periodic doubling bifurcation is given Figure 3.8.
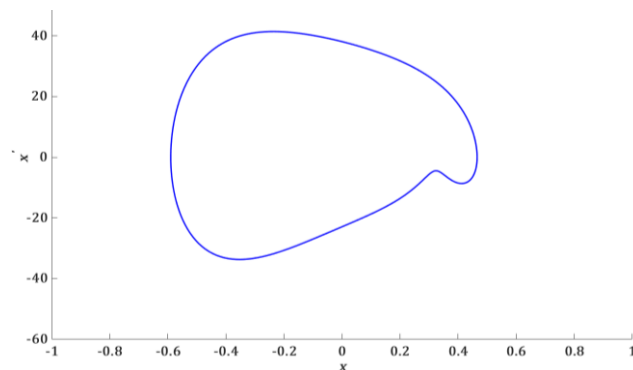
Figure 3.8. Periodic doubling phase diagram

3.2.3   MATCONT

The development of MATCONT started in 2000 and published its first version in 2003 by Dr. Willy Govaerts, Prof. Yuri A. Kuznetsov and Dr. Bart Sautois [42]. MATCONT is a MATLAB package and can work only MATLAB installed computers. The package provides bifurcation analysis, time integration, vector fields and maps, numerical continuation, periodic and homoclinic orbits and normal form analysis.

MATCONT can be used via GUI or MATLAB files manually. The GUI includes three main windows; the main window where ODEs can be defined, analysis type can be chosen and graphs can be created. In "Starter" window, one can select the bifurcation types to be found, define initial point, continuation and discretization parameters. In "Continuer" window the step size, error tolerances and maximum number of point to be calculated can be defined. Another window, "Integrator" will pop up when time integration is selected in main window. Time integration parameters such as solver, step size, error tolerance and time interval to be integrated are defined in "Integrator" window.

MATCONT is able to locate bifurcations such as Hopf, pitchfork, limit cycle, period doubling and fold bifurcations. The package provides also normal form coefficients and eigenvalues of the system at varying system parameters. The stability analysis of limit cycle can be performed with Lyapunov coefficients. The Poincare maps can be created for further investigation. The locations of bifurcations are conducted using test functions which are specialized for a certain types of bifurcations.

4.   EIGENVALUE ANALYSIS OF LINEAR AEROELATIC MODEL

The AEOM was transformed into a matrix form in the section 2.3[th] section as given in Eq. 4.1. The physical properties of the 3 DOFs wing and control surface is taken from [27] and given in Table 4.1.

$$Q = \begin{bmatrix} -(A+\rho B)^{-1}(C+\rho U D) & -(A+\rho B)^{-1}(E+\rho U^2 F) & -(A+\rho B)^{-1}(\rho U^3 W) \\ I_{3\times3} & 0_{3\times3} & 0_{3\times6} \\ 0_{6\times3} & W_1 & U W_2 \end{bmatrix} \qquad 4.1$$

Table 4.1. The physical properties of the airfoil

m	Total mass (kg)	3.391
l	Length of span (m)	0.52
I_α	mass moment inertia around x_f (kg.m^2)	1.347e-2
S_α	static mass moment around x_f (kg.m)	8.587e-2
I_β	mass moment inertia around x_h (kg.m^2)	3.264e-4
S_β	static mass moment around x_h (kg.m)	3.95e-3
$I_{\alpha\beta}$	product of mass moment inertia kg.m^2	8.280e-04
x_f	the position of elastic axis of wing (m)	0.0635
x_h	The position of elastic axis of control surface (m)	0.1905
c	the length of airfoil (m)	0.254
K_h	Stiffness in plunge direction (N/m)	2818.8
K_α	Stiffness in pitch direction (N.m/rad)	37.3
K_β	Stiffness in control direction (N.m/rad)	3.9175
C_h	Modal damping in plunge direction (N.s/m)	0.0113
C_α	Modal damping in pitch direction (N.m.s/rad)	0.01626
C_β	Modal damping in control direction (N.m.s/rad)	0.0115
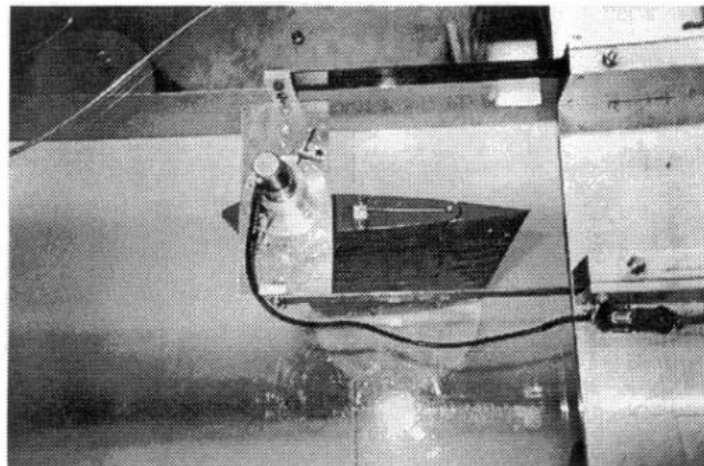
Figure 4.1 Conner's experimental setup

The eigenvalues of AEOM is obtained solving characteristic equation. The solution of characteristic equation is handled using *eig( )* command of MATLAB. The eigenvalues and eigenvectors are calculated at various airspeeds. The natural frequencies of the structure are found as 4.443 Hz, 9.206 Hz and 19.482 Hz.

At the airspeed equals $U_F = 23.98$ m/s the total damping of the pitching mode crosses the zero line. The frequency of the flutter motion is $\omega_F = 6.06\ Hz$. The change of damping and frequency of the system with varying airspeed is given in Figure 4.2.
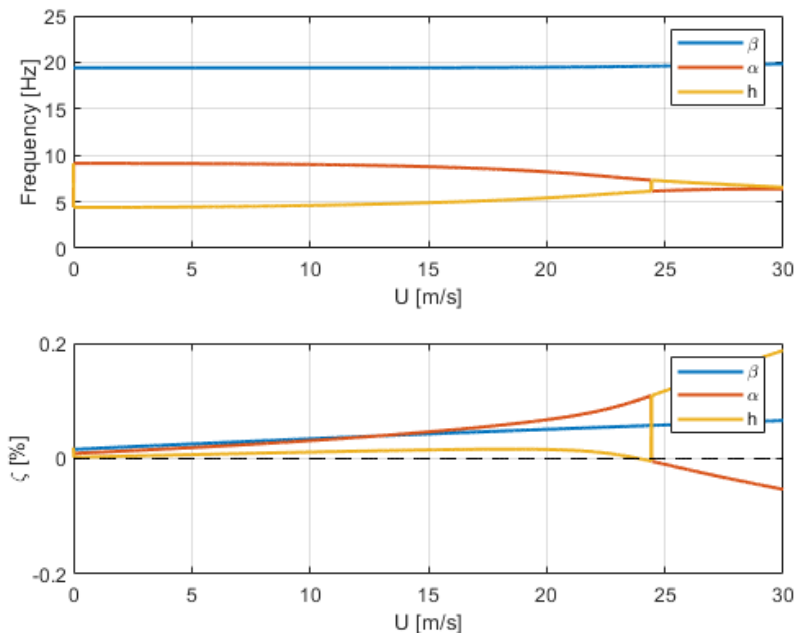
Figure 4.2. Air speed vs. frequency and air speed vs. damping

The comparison of the results with respect to referenced article is given in the Table 4.2. The errors are calculated relative to the experimental results. The results are in agreement with both experimental and numerical results of the reference. The difference between wind tunnel test and numerical solutions can be related to the aerodynamics effect that cannot be calculated with potential theory.

Table 4.2. Comparison of the results

	Present Study	Conner (Numerical)	Conner (Experimental)	Error[%]
U_F	23.98 m/s	23.9 m/s	20.6 m/s	16.41
ω_F	6.06 Hz	6.112	5.47	10.786
ω_h	4.443 Hz	4.455	4.375 Hz	1.554
ω_α	9.206 Hz	9.218 Hz	9.125 Hz	0.888
ω_β	19.482 Hz	19.442	18.625 Hz	4.601

The time responses of the system are calculated using *ode45* MATLAB's Runge – Kutta 5th order time integration method. The time responses are calculated at the airspeeds; 23 m/s, 23.98 m/s and 24.1 m/s and given in Figure 4.3. As one can see in upper left response at Figure 4.3, the damping is high enough to damp the system response. But in the upper right response, time responses do not change with the time. As mentioned earlier, this phenomenon is called limit cycle oscillation or LCO. The airspeed where LCO occurs is called Hopf speed, U_H in nonlinear systems. In the bottom figure, time responses of the system increases with time for linear system this phenomenon is called flutter.
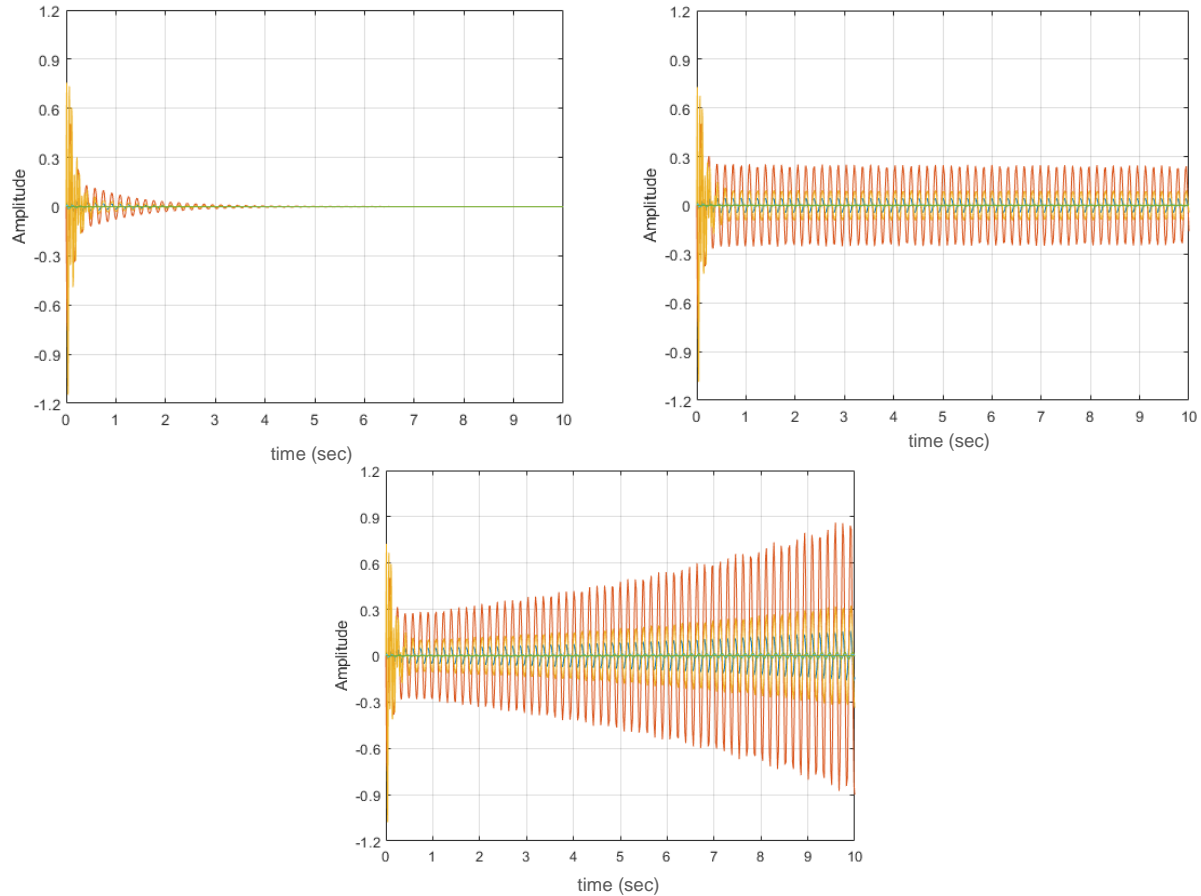
Figure 4.3. Time responses of 3 DOF system at $23, 23.9$ and $24\ m/s$ airspeeds

5. ANALYSIS OF LINEAR MODEL IN ZAERO

ZAERO is widely used software in the field of aeroelasticity. The software is used for flutter, aeroservoelasticity, transient gust, maneuver, trim and ejection load analysis. The software uses different type of aerodynamic modeling methods according to Mach speed. ZONA06 is used for subsonic speed which is a higher order paneling scheme compared to DLM. The difference in the order of the panel element can be shown in Figure 5.1. The higher order element of ZONA06 provides more robust solution due to the efficient modeling with fewer elements compared to DLM.
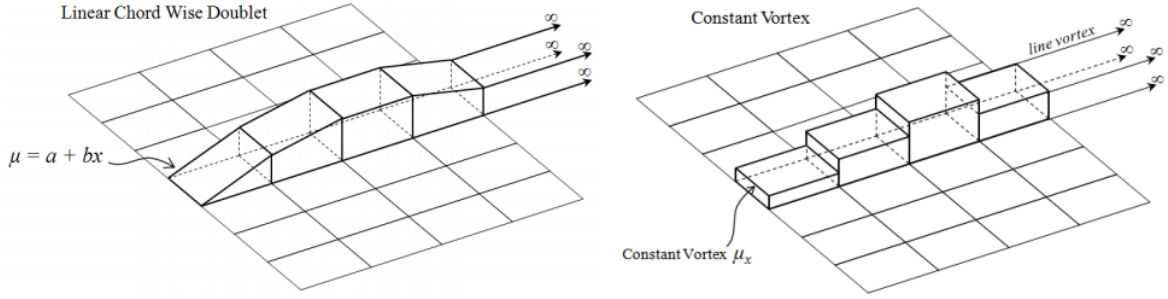
Figure 5.1. The panel element order difference between ZONA06 and DLM [43].

The ZAERO results will be obtained to compare results from abovementioned linear analysis method to check consistency with the numerical results. Before presenting the results, mentioning about the modeling methods and mathematical background of the software would create understanding. In the following paragraphs, for the theoretical background of ZAERO, ZAERO User Manual 9.3 and Theoretical Manual 9.3 are greatly benefited.

5.1. Mathematical Background of Aeroelasticity in ZAERO

As mentioned before, aeroelasticity is the field of engineering that investigates the interactions of a body in the aspects of aerodynamic, dynamic and elasticity. The aeroelastic equation of motion for discrete system is given in general form as follows:

$$\overline{M}\ddot{x} + \overline{K}x = F(t) \tag{5.1}$$

The force vector can be defined as summation of structural and aerodynamic forces such as

$$F(t) = F_a(x) + F_e(t) \tag{5.2}$$

where $F_e(t)$, is external forces and depends on a given input such as control surface command, ejection of a store or unwanted aerodynamic forces such as gusts. $F_a(x)$ is the aerodynamic force that depends on the structural deformation which causes deflection in aerodynamic surfaces and changes aerodynamic force vector. The relation of this coupling is represented as aerodynamic feedback in the Theoretical Manual of ZAERO v9.3 and given in Figure 5.2.
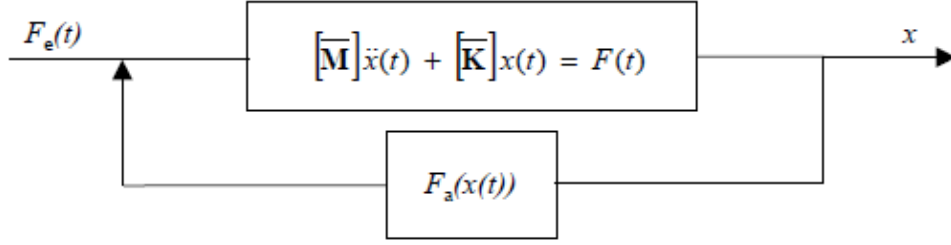
Figure 5.2. Aerodynamic Function Diagram [44]

The introduction of $F_a(x)$ eliminates the above equation becoming a forced vibration equation so that the new form of Eq. 5.1 can be rearranged as follows.

$$\overline{M}\ddot{x} + \overline{K}x - F_a(x) = F_e(t) \qquad 5.3$$

As the flutter is a self-excited phenomenon the external forces defined in Eq. 5.3 is not necessary any further and new form of the equation is given below

$$\overline{M}\ddot{x} + \overline{K}x - F_a(x) = 0 \qquad 5.4$$

If the force $F_a(x)$ is nonlinear, the eigenvalue solution is not valid anymore and time-marching methods must be used for solution. However, it is also possible to approximate to linear system by linearizing the amplitudes which makes possible to use complex eigenvalue solutions method and become stability problem once again. The amplitude linearization is valid if the perturbation is small enough at all air speeds. A transfer function can be defined for the assumed linear model. The abovementioned aerodynamic feedback mechanism relates $F_a(x)$ and x using convolution integral as follows.

$$F_a(x) = \int_0^t q_\infty H(\frac{U}{b}(t - \tau)x(\tau)d\tau \qquad 5.5$$

The term H represents the aerodynamic transfer function and it can be transformed into Laplace domain which is given in the following equation.

$$F_a(x(s)) = q_\infty \overline{H}\left(\frac{sb}{U}\right)x(s) \qquad 5.6$$

where $\overline{H}$ is the Laplace domain counterpart of H.

The aeroelastic equation of motion in Laplace domain is defined as below where M and K are generalized mass and stiffness matrix and q_∞ is dynamic pressure.

$$\left[s^2\bar{M} + \bar{K} - q_\infty\bar{H}\left(\frac{sb}{U}\right)\right]x(s) = 0 \qquad 5.7$$

The solution of eigenvalues in physical coordinates is a cumbersome, so that, the solution is obtained in the modal coordinates. The displacements can be transformed from one to another using modal matrix, $\boldsymbol{\Phi}$ such as

$$x = \boldsymbol{\Phi}q \qquad 5.8$$

where $\boldsymbol{q}$ is the displacement in modal coordinates or generalized coordinates. The substitution of Eq. 5.8 into 5.7 and pre-multiplication of Eq. 5.7 with the transpose of modal matrix, $\boldsymbol{\Phi}^T$ gives the following aeroelastic equation of motion

$$\left[s^2\boldsymbol{M} + \boldsymbol{K} - q_\infty\boldsymbol{Q}\left(\frac{sb}{U}\right)\right]q = 0 \qquad 5.9$$

The matrices $\boldsymbol{M}$, $\boldsymbol{K}$ and $\boldsymbol{Q}$ are generalized forms of mass, stiffness and aerodynamic force matrices and given as follows

$$\mathbf{M} = \boldsymbol{\Phi}^T\bar{M}\boldsymbol{\Phi} \qquad 5.10$$

$$\mathbf{K} = \boldsymbol{\Phi}^T\bar{K}\boldsymbol{\Phi} \qquad 5.11$$

$$\mathbf{Q}\left(\frac{sb}{U}\right) = \boldsymbol{\Phi}^T\bar{H}\left(\frac{sb}{U}\right)\boldsymbol{\Phi} \qquad 5.12$$

The solution of Eq. 5.9 in Laplace domain is not efficient due to the complexity of unsteady aerodynamics. For this reason, the formulation of unsteady aerodynamics in frequency domain with the assumption of simple harmonic motion provides more efficient solutions. The aerodynamic transfer function that defined in frequency domain is called Aerodynamic Influence Coefficient (AIC) matrix.

Each element in panel method are called as aerodynamic boxes, have control points where the boundary conditions are defined. In panel method, the integration on control points and summation of these integrals gives a matrix whose coefficients resembles the aerodynamic

influences at control points of each boxes. This matrix is called as Aerodynamic Influence Coefficients as it is mentioned before where it defines relationship between structural deformation and aerodynamic forces as defined in following equation.

$$F_h = q_\infty [AIC(ik)]h \qquad 5.13$$

where F_h aerodynamic forces as a result of structural deformation h at the aerodynamic boxes,. The AIC matrix is computed in the reduced frequency domain which is defined as

$$k = \frac{\omega b}{U} \qquad 5.14$$

where ω is harmonic oscillation frequency, b is the reference length of aerodynamic surface, U is undisturbed airspeed. The AIC matrix defines the relation between structural deformation and aerodynamic forces where AIC is calculated on the control points of aerodynamic boxes whose coordinates differs from grid points of structural model. The spline method accomplishes this forces and displacements transferal using interpolation from grid points to aerodynamic control points of panels. The spline method will be explained in the following paragraphs.

5.2.   Spline

The force and displacement coupling between structural and aerodynamic model is accomplished with the spline method. The displacement transfer is performed from structural grid point of finite element (FE) model to control points of aerodynamic boxes and force displacement is performed from control points of aerodynamic boxes to grid points of structural model.

The position difference between structural grid points and aerodynamic control points must be small for accomplishing interpolation from structural component to aerodynamic surfaces accurately. This transfer is accomplished using spline matrix, G such that:

$$h = Gx \qquad 5.15$$

where **h** is defined as aerodynamic control points and x is defined as structural grid point in finite element model. The generated spline matrix transfers the forces from aerodynamic control points to structural grid points as shown below:

$$F_a = G^T F_h \qquad\qquad 5.16$$

The spline method is founded on the virtual work principle. Since the work done by aerodynamic forces must equal to structural forces, one can define using virtual displacement:

$$\delta h^T F_h = \delta x^T F_a \qquad\qquad 5.17$$

After substitution of Eq. 5.15 into 5.17 and rearranging the outcome, the following equation is obtained.

$$\delta x^T (F_a - G^T F_h) = 0 \qquad\qquad 5.18$$

where δx cannot be zero due to the randomness of virtual displacement, Eq. 5.16 is obtained. The substitution of Eq. 5.13 and 5.15 into Eq. 5.16 yield the following equation.

$$F_a = q_\infty G^T [AIC(ik)] Gx \qquad\qquad 5.19$$

The generalized form of aerodynamic forces can be obtained using the same procedure as used in acquiring modal mass, stiffness and transfer function.

$$Q(ik) = \Phi^T G^T [AIC(ik)] G\Phi \qquad\qquad 5.20$$

As mentioned before, ZAERO solves the flutter problem in the frequency domain with the assumption of simple harmonic motion. The frequency domain form of Eq.5.9 can be represented as follows

$$[-\omega^2 M + K - q_\infty Q(ik)]q = 0 \qquad\qquad 5.21$$

5.3. Mathematical Background of Flutter Solutions in ZAERO

In ZAERO the flutter analysis can be performed with using multiple methods such as; g-method, k-method and p-k method. For the p-k method, the explanation of p method is necessary. The differences of these methods are briefly explained in following parts.

5.3.1   p-Method

The p-method uses Laplace parameter, p, which is introduced as follows

$$p = \frac{sb}{U} = (\gamma k + ik) \qquad 5.22$$

Where k is reduced frequency and defined as $k = \frac{\omega b}{U}$, and γ is transient decay coefficient. After substituting Eq. 5.22 into 5.9, the new equation is obtained and called as p-method.

$$\left[\left(\frac{U}{b}\right)^2 Mp^2 + K - q_\infty Q(p)\right]q = 0 \qquad 5.23$$

Since the p-method solution provides true damping yet the complicated solution of unsteady aerodynamics in the Laplace domain makes the p-method inefficient. ZAERO uses mostly reduced frequency domain methods for flutter solution.

5.3.2   k-Method

ZAERO performs flutter analysis in frequency domain with assumption of simple harmonic motion. The substitution of $Q\left(\frac{sb}{U}\right)$ in Eq. 5.9 with $Q(ik)$ and s with $i\omega$ will give the following equation.

$$[-\omega^2 M + K - q_\infty Q(ik)]q = 0 \qquad 5.24$$

An artificial damping is added into Eq. 5.24 and the final form is given in 5.25 where g is artificial structural damping which was firstly introduced by Theodorsen for providing harmonic motion. The k-method is able to calculate flutter points at zero damping however a reliable damping prediction is essential for flight flutter test. For these reasons, another method p-k method is frequently used for obtaining flutter boundary.

$$[-\omega^2 M + (1 + ig_s)K - q_\infty Q(ik)]q = 0 \qquad 5.25$$

The equation that is given in Eq. 5.25 is so-called k-method. To transform the above equation into complex eigenvalue problem the dynamic pressure can be derived as follows

$$q_\infty = \frac{1}{2}\rho U^2 = \frac{1}{2}\rho \left(\frac{\omega b}{k}\right)^2 \qquad 5.26$$

where ρ is the air density. After substituting Eq. 5.26 into 5.25 and dividing to ω^2 will give the following equation:

$$\left[\boldsymbol{M} - \lambda \boldsymbol{K} - \frac{1}{2}\rho \left(\frac{b}{k}\right)^2 \boldsymbol{Q}(ik) \right] \boldsymbol{q} = \boldsymbol{0} \qquad 5.27$$

where

$$\lambda = \frac{(1 + ig_s)}{\omega^2} \qquad 5.28$$

which is the complex eigenvalue of Eq. 5.25. The existence of the rigid body modes makes the solution more challenging due to the requirement of trivial solution. So that, it is required to eliminate the trivial solution by partitioning in Eq.5.27 as rigid body and elastic modes:

$$\left[\begin{bmatrix} \boldsymbol{M}_{RR} & \boldsymbol{0} \\ \boldsymbol{0} & \boldsymbol{M}_{EE} \end{bmatrix} + \frac{1}{2}\rho \left(\frac{b}{k}\right)^2 \begin{bmatrix} \boldsymbol{Q}_{RR} & \boldsymbol{Q}_{RE} \\ \boldsymbol{Q}_{ER} & \boldsymbol{Q}_{EE} \end{bmatrix} - \lambda \begin{bmatrix} \boldsymbol{0} & \boldsymbol{0} \\ \boldsymbol{0} & \boldsymbol{K}_{EE} \end{bmatrix} \right] \begin{Bmatrix} \boldsymbol{q}_R \\ \boldsymbol{q}_E \end{Bmatrix} \qquad 5.29$$

where subscripts R and E denote rigid body and elastic modes. The rigid body displacement can be written as follows

$$\{\boldsymbol{q}_R\} = -\overline{\boldsymbol{M}}_{RR}^{-1} \overline{\boldsymbol{M}}_{RE} \{\boldsymbol{q}_E\} \qquad 5.30$$

The AEOM that is given in 5.29 can be reduced as given below

$$\left[\left[-\overline{\boldsymbol{M}}_{ER} \overline{\boldsymbol{M}}_{RR}^{-1} \overline{\boldsymbol{M}}_{RE} + \overline{\boldsymbol{M}}_{RE} \right] - \lambda [\boldsymbol{K}_{EE}] \right] \{\boldsymbol{q}_E\} = 0 \qquad 5.31$$

where

$$\overline{\boldsymbol{M}}_{ER} = \frac{1}{2}\rho \left(\frac{b}{k}\right)^2 \boldsymbol{Q}_{ER}$$

$$\overline{\boldsymbol{M}}_{RR} = \boldsymbol{M}_{RR} + \frac{1}{2}\rho \left(\frac{b}{k}\right)^2 \boldsymbol{Q}_{RR}$$

$$\qquad \qquad \qquad \qquad \qquad \qquad \qquad \qquad \qquad \qquad 5.32$$

$$\overline{\boldsymbol{M}}_{RE} = \frac{1}{2}\rho \left(\frac{b}{k}\right)^2 \boldsymbol{Q}_{RE}$$

$$\overline{\boldsymbol{M}}_{EE} = \boldsymbol{M}_{EE} + \frac{1}{2}\rho \left(\frac{b}{k}\right)^2 \boldsymbol{Q}_{EE}$$

The solution for λ at different reduced frequencies and aerodynamic conditions will give the flutter solution. The damping and frequencies for each structural mode as the airspeed changes can be calculated as follows

$$\omega_f = \frac{1}{\sqrt{Re(\lambda)}}$$

$$g_s = \frac{Im(\lambda)}{Re(\lambda)} \qquad\qquad 5.33$$

$$U_f = \frac{\omega_f b}{k}$$

The flutter occurs where the damping crosses the zero line as mentioned in the linear solution method in the 3th section. The frequencies and air speeds are evaluated at defined Mach and air density. The flutter solution is called matched if U_f equals multiplication of Mach number, M and sound of speed, a_∞ at the given air density otherwise it is called non-matched flutter solution. The flutter solution must be evaluated at different airspeed to obtain matched solution where $U_f = Ma_\infty$.

5.3.3   p-k Method

The aeroelastic equation of p-k method is derived using both p and ik terms that given in p and k methods and become as follows

$$\left[\left(\frac{U}{b}\right)^2 \boldsymbol{M}p^2 + \boldsymbol{K} - \frac{1}{2}\rho U^2 \boldsymbol{Q}(ik)\right]\{\boldsymbol{q}\} = \boldsymbol{0} \qquad\qquad 5.34$$

The p-k method uses complex eigenvalue solution at defined values of U and q_∞ that alters the value of p. It is necessary to obtain matched solution for the reduced frequency with the imaginary part of p. For simplicity, the damping term, g_s is omitted and embedded into the p term as shown below

$$p = (g + ik) \qquad\qquad 5.35$$

since

$$g = \gamma k \qquad\qquad 5.36$$

where γ is transient decay coefficient. The p-k method has mathematical inconsistency due to the expression of eigenvalue p as a damped sine where $\boldsymbol{Q}(ik)$ is defined as undamped sine harmonic yet it is proofed as a good approximation of p-method. The structural damping added form of Eq. 5.34 was derived by Rodden [45] and given as below

$$\left[\left(\frac{U}{b}\right)^2 \boldsymbol{M}p^2 + \boldsymbol{K} - \frac{1}{2}\rho U^2 \frac{Im\big(\boldsymbol{Q}(ik)\big)}{k}p - \frac{1}{2}\rho U^2 \frac{Re\big(\boldsymbol{Q}(ik)\big)}{k}\right]\{\boldsymbol{q}\} = \boldsymbol{0} \qquad 5.37$$

Substituting Eq. 5.35 into Eq. 5.37 and rewrite the equation will give

$$\left[\left(\frac{U}{b}\right)^2 \boldsymbol{M}p^2 + \boldsymbol{K} - \frac{1}{2}\rho U^2 \frac{Im\big(\boldsymbol{Q}(ik)\big)}{k}g - \frac{1}{2}\rho U^2 \boldsymbol{Q}(ik)\right]\{\boldsymbol{q}\} = \boldsymbol{0} \qquad 5.38$$

The extra term compared to Eq. 5.34 is defined as aerodynamic damping matrix which is stated as follows

$$-\frac{1}{2}\rho U^2 \frac{Im\big(\boldsymbol{Q}(ik)\big)}{k}g$$

The AEOM is solved at given values of airspeed, U and air density, ρ for complex eigenvalue p which is related with the mode of interest. The solution for p is accomplished with iterative solution process when the iterated reduced frequency is matched with the imaginary part of p for each structural modes which also requires consecutive interpolations for defined reduced frequencies.

5.3.4   g-Method

The g-Method is developed as a newly flutter solution method by ZONA Technology that is generalizing k-method and p-k method for better damping estimation. The p-k method could produce unrealistic damping values when the generalized aerodynamic forces are highly nonlinear.

The matched point flutter solutions are performed using g-methods in ZAERO. The software has its own standard atmosphere table, where air density changes with altitude.

The g-method consists damping of first order which is derived from Laplace domain aerodynamics. The assumption of Eq. 5.39 is analytic in the interval of $g \geq 0$ and $g < 0$ is the foundation of g-method.

$$Q(p) = Q(g + ik) \qquad 5.39$$

The term $Q(p)$ can be expanded on the imaginary axis by assuming $g = 0$. The expansion of $Q(p)$ is given as follows

$$Q(p) \approx Q(ik) + g \left. \frac{\partial Q(p)}{\partial g} \right|_{g=0} \qquad 5.40$$

The assumption of $Q(p)$ is analytic gives chance to apply Cauchy-Riemann rule on the partial derivative part of the above equation and given as follows

$$\frac{\partial Re(Q(p))}{\partial g} = \frac{\partial Im(Q(p))}{\partial k}$$
$$\frac{\partial Im(Q(p))}{\partial g} = -\frac{\partial Re(Q(p))}{\partial k} \qquad 5.41$$

Summation of first equation with i multiplied second equation gives the following result

$$\frac{\partial Q(p)}{\partial g} = \frac{\partial Q(p)}{\partial (ik)} \qquad 5.42$$

The above equation is valid through the p-domain except along the real negative axis due to continuity changes. So that the term $\left. \frac{\partial Q(p)}{\partial g} \right|_{g=0}$ can be replaced with

$$\left. \frac{\partial Q(p)}{\partial g} \right|_{g=0} = \left. \frac{\partial Q(p)}{\partial (ik)} \right|_{g=0} = \frac{\partial Q(ik)}{\partial (ik)} = Q(ik)' \qquad 5.43$$

The final form of 5.40 can be represented as follows

$$Q(p) \approx Q(ik) + gQ(ik)' \qquad 5.44$$

The final form of AEOM can be obtained substituting the Eq. 5.44 into Eq. 5.23 which is given in below

$$\left[\left(\frac{U}{b} \right)^2 Mp^2 + K - \frac{1}{2}\rho U^2 Q(ik)'g - \frac{1}{2}\rho U^2 Q(ik) \right] \{q\} = 0 \qquad 5.45$$

The comparison of the final form of AEOM in g-method and p-k method shows that if the damping value, g is zero both equations become identical. The solution of above equation is briefly explained in following part. The substitution of $g + ik$ into p in the Eq. 5.45 gives the following equation

$$[g^2 A + g B - C]\{q\} = 0 \qquad 5.46$$

where:

$$
\begin{aligned}
A &= \left(\frac{U}{b}\right)^2 M \\
B &= 2ik\left(\frac{U}{b}\right)^2 M - \frac{1}{2}\rho U^2 Q(ik)' + \left(\frac{U}{b}\right) Z \qquad 5.47 \\
C &= -k^2\left(\frac{U}{b}\right)^2 M + K - \frac{1}{2}\rho U^2 Q(ik) + ik\left(\frac{U}{b}\right) Z
\end{aligned}
$$

The term Z is modal structural damping matrix. In the above equation flutter speed can be obtained when the imaginary part of g becomes zero. The g-Method equation that is given the Eq. 5.45 is second order linear system and its solution can be completed when the abovementioned criteria is met. The Eq. 5.45 can be rewritten in the form of eigenvalue problem and solved for eigenvalues at several reduced frequencies. The eigenvalue problem and eigen solution of Eq. 5.45 can be shown as follows

$$[D - gI]\{X\} = 0 \qquad 5.48$$

where X is the eigenvector and D is given as below

$$D = \begin{bmatrix} 0 & I \\ -A^{-1}C & -A^{-1}C \end{bmatrix} \qquad 5.49$$

5.4. Aeroelastic Analysis Setup in ZAERO

ZAERO uses scripts as an input where the airspeed, geometry, FE results and spline data are entered manually. The inputs in ZAERO are classified as *"Executive Control Section"* and *"Case Control Section"*. In the first section, finite element results file and the symmetry conditions are defined. In the second section, the solution method, airspeed,

49

geometry inputs, spline, structural damping can be defined. The important case control commands are briefly explained in the following paragraphs.

The aerodynamic surfaces that generate lift are defined with the CAERO7 and the surfaces that will not generate lift are defined with the BODY7 bulk data card. The spline is generated with SPLINE0, SPLINE1, SPLINE2 and SPLINE3 bulk data cards. Each spline bulk data card uses different spline theorem. In this work, SPLINE1 bulk data card is used which uses infinite plate spline method. Infinite plate spline theory is based on the idea of 2D interpolation. A working plane is defined as the lifting surface plane. This makes infinite plate spline more suitable for wing-like geometries.

MKAEROZ bulk data card is used for defining airspeed and the reduced frequencies that is going to be swept. For each airspeed, an AIC matrix is generated and saved which can be used for different finite element results of same geometry and spline and obtain faster results for iterative works. FLUTTER bulk data card is used for defining the input for flutter or aeroservoelastic analysis. In this card, the structural damping, symmetry condition and number of modes can be defined for flutter analysis. The FIX label in the FLUTTER bulk data card, defines the solution type for flutter. In this work, FIXDEN bulk data card is used for solution which activates k-method solution procedure and is a non-matched method which is the same solution procedure that used in the eigenvalue analysis above.

5.4.1 The Panel Model

The experimental model is created using CAERO7 bulk data card. The geometry of airfoil section is not represented when using panel method due to its negligible effects. The thickness effect on lifting surface is first order for unsteady linear aerodynamics that gives the possibility of modeling lifting surfaces as flat plate. The source and doublet singularities that are present on the flat plate are used for simulating the thickness effects and generating lift. However since the typical section method is valid and gives better results for higher aspect ratios. The new aspect ratio for the model is defined as 100. The

image of the model with aspect ratio of 100 would be too thin to share here. So that the symbolic panel model of the experimental setup is given in Figure 5.3.
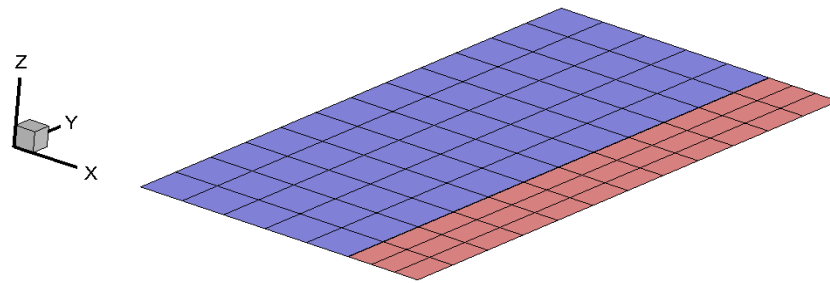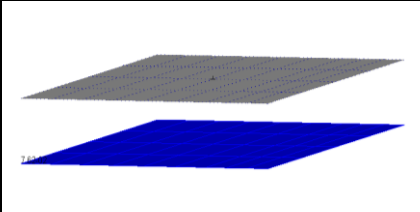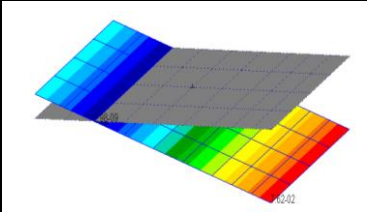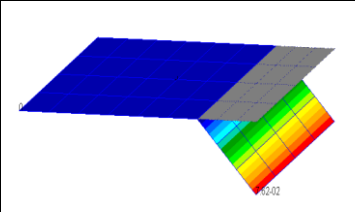

Figure 5.3. The aerodynamic paneling of the 2D system

5.4.2   Modal Analysis Results

The mass normalized mode shapes that are obtained from the modal analysis that is given above is used as inputs for the ZAERO analysis. The mode shapes of the system are visualized using MSC Patran. The mode shapes and the natural frequencies of the model are given in Table 5.1. The first mode shape of the system shows plunge motion, the second mode shape shows pitching motion. Finally the third mode shows control surface motion.

Table 5.1. Finite Element Results of 3D wing-control surface system

Mode 1 @4.444 Hz	Mode 2 @9.23 Hz	Mode 3 @19.334Hz

5.5.   ZAERO Results

The flutter analyses are performed at the varying and airspeed. The airspeeds are given in Table 5.2.

Table 5.2. Airspeeds

#	1	2	3	4	5	6	7	8	9
[m/s]	5	8	10	15	20	21	22	22.5	23
	10	11	12	13	14	15			
[m/s]	24	24.5	25	30	35	40			

The frequency-airspeed and damping – airspeed diagram are obtained using the output file of ZAERO and given in Figure 5.4. The frequency-airspeed and damping – airspeed diagram from eigenvalue solution of linear system are given in Figure 5.5 for comparing results from both solutions.
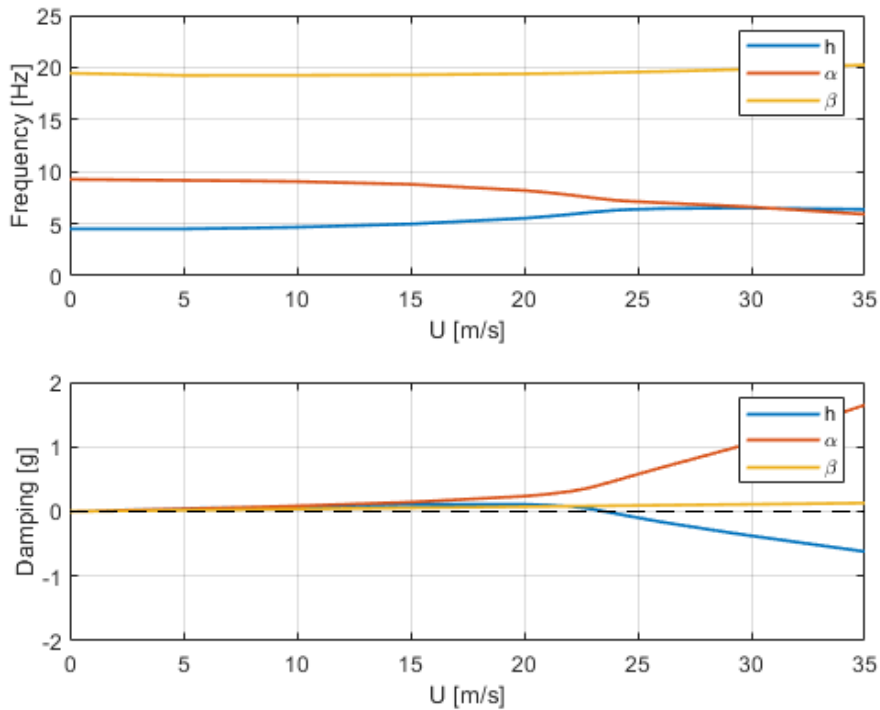

Figure 5.4. The change of frequency and damping with respect to airspeed (ZAERO)
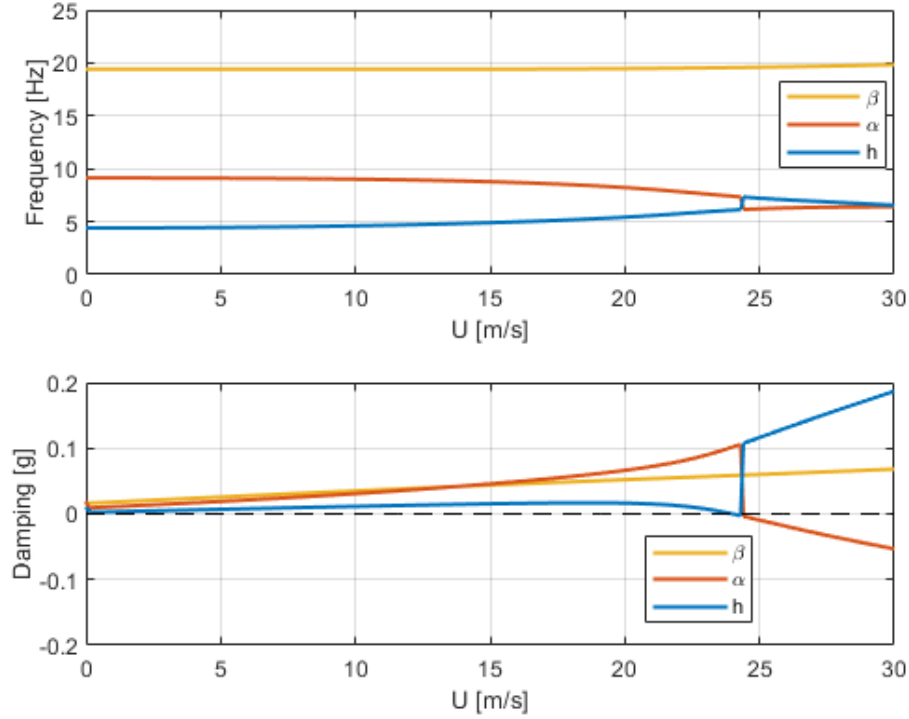
Figure 5.5. The change of frequency and damping with respect to airspeed

Table 5.3. Comparison of the results

	Present Study (Numerical)	Present Study (ZAERO)	Conner (Experimental)	Error[%] Numerical	Error[%] ZAERO
U_F	23.98 m/s	23.55 m/s	20.6 m/s	16.41	14.27
ω_F	6.06 Hz	6.20 Hz	5.47 Hz	10.786	13.35

In ZAERO, the flutter speed and flutter frequency are calculated at 23.55 m/s and 6.20 Hz at sea level. The flutter speed and flutter frequency were calculated using eigenvalue solution at 23.98 m/s and 6.06 Hz at sea level. The errors for the flutter frequency and flutter airspeed are compared in the Table 5.3. The ZAERO and numerical solution in this study is consistent with Conner's numerical results.

As mentioned above, the typical section gives more accurate results at high aspect ratios. So that to compare the results with typical section results the ZAERO model rearranged for

high aspect ratio value of 100. Another model with the original dimensions is analyzed in ZAERO and it is seen that flutter speed and frequency of this model is higher compared to model that have higher aspect ratio.

6. ANALYSIS OF NONLINEAR MODELS

The nonlinear model is obtained via introducing nonlinear structural elements into the equation of motion of linear system. The MATLAB software is used for acquiring the nonlinear AEOM using symbolic math tool. Each nonlinearity analyses are given in separate sections. In the first section, cubic stiffness defined for each degree of freedom. In the second section, the quadratic damping is introduced for pitching degree of freedom. Finally, the free-play nonlinearity is also introduced into pitching direction.

The stability of the limit cycles is assigned according to the types of bifurcation. For more complex bifurcation diagrams with more than one branch, the test functions and Lyapunov coefficients are investigated to decide whether the limit cycle is stable or unstable.

6.1. Cubic Stiffness Nonlinearity Analyses

6.1.1 Cubic Nonlinearity Analysis in Pitching Direction

In this section, the cubic stiffness, K_{α_3} in pitching direction defined with the multipliers of 10 of the linear stiffness in pitching direction. The new AEOM with nonlinearity in pitching direction is given in Eq. 6.1

$$\dot{x} = Qx + K_{\alpha_3} q \alpha^3 \qquad 6.1$$

where Q is the aeroelastic equation of motion that is obtained in Section 2.3 and given with Eq. 2.23, q is the forcing vector and given as follows

$$q = \left[\begin{array}{c} -(A + \rho B)^{-1} \begin{bmatrix} 0 \\ 1 \\ 0 \end{bmatrix} \\ \mathbf{0}_{9 \times 1} \end{array} \right] \qquad 6.2$$

The MATCONT form of the nonlinear AEOM has a varying parameter which is the airspeed U. In MATCONT, the first step is to find equilibrium points. The equilibrium points can be found after initial parameters are chosen. The initial parameters are $U = 23.0 \, m/s$ for airspeed and $K_{\alpha_3} = 10 \times K_\alpha = 373 \frac{Nm}{rad}$.

The first bifurcation point is achieved at the airspeed $U = 23.98 \, m/s$ as a Hopf bifurcation. The nonlinear analysis continues with choosing the Hopf point as a starting airspeed to obtain response of the nonlinear aeroelastic system. After selection of initial point and the initial conditions of the system and the system parameters that are going to be tracked are selected. The airspeed and the period of the oscillation are chosen as the varying parameters during the continuation while cubic stiffness remains constant.

The limit cycle amplitudes of each state and the periods are calculated at varying airspeeds. The results of the analysis are given with the assumption of the structure withstand excessive deformations. The phase plane change with varying airspeeds for the pitching direction is given in Figure 6.1 which consist the airspeed U on X axis, the rotation α at Y axis and derivative of the rotation $d\alpha$ at Z axis. The projection of the results on XY plane gives Figure 6.2. In this analysis, two limit point cycles (LPC), two Neutral Saddle points (NS), and two branch points of cycles (BPC) are obtained and stated in the figures. The maximum values of limit cycles are obtained for pitching motion and given in Figure 6.2. The figures that shows the response of a system with respect parameter change is called as bifurcation diagrams. As shown in bifurcation diagram, one can find out the following outcomes. First of all, in the presence of the cubic stiffness nonlinearity, more benign behavior can be observed compared to linear system. As it can be seen with the increasing airspeed, the system response shows much less amplitude than any divergent situation as would be in the linear system.
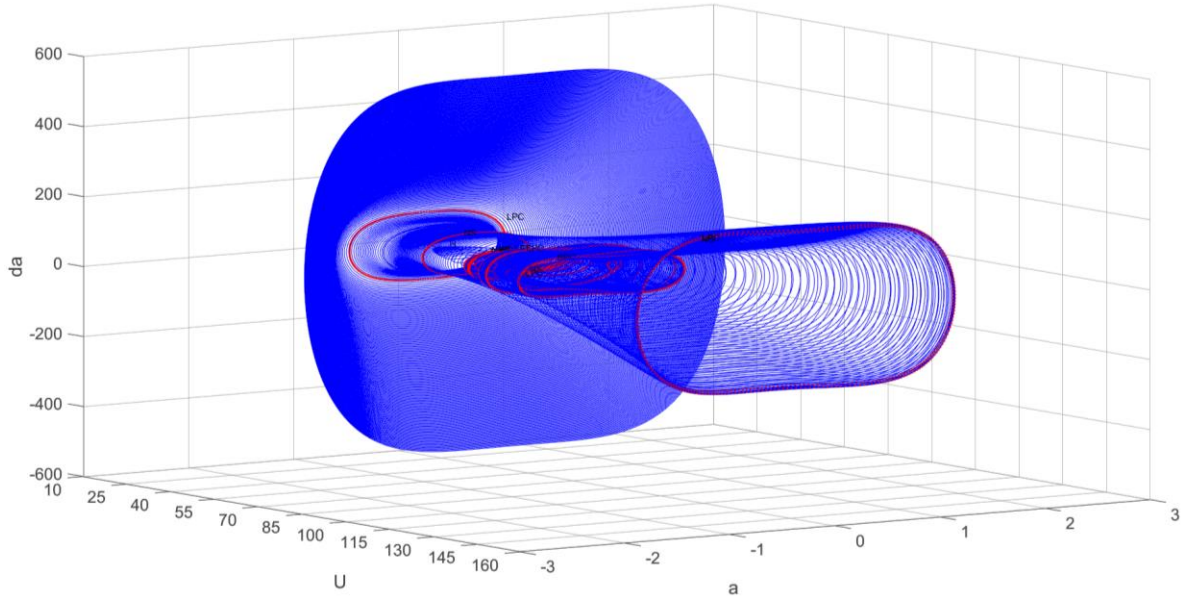
Figure 6.1. The cubic stiffness results for $K_{\alpha_3} = 373 \frac{Nm}{rad}$
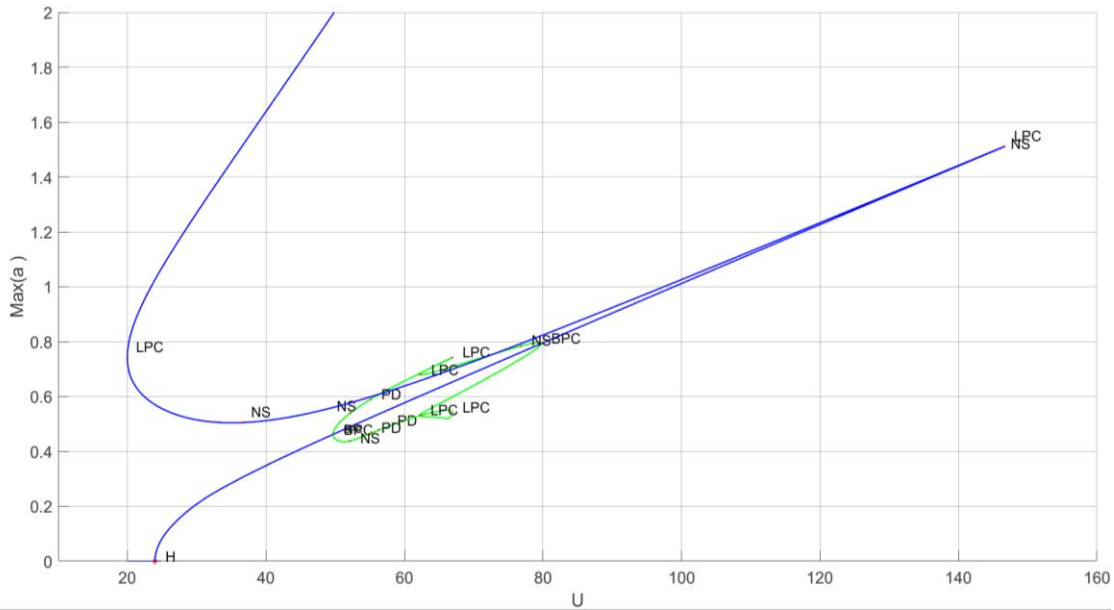

Figure 6.2. The bifurcation diagram for pitching response α for $K_{\alpha_3} = 373 \frac{Nm}{rad}$

The LPC points which can be stated as fold bifurcation as well which are found at the turning points along the line. As mentioned before, the fold bifurcation creates stable and unstable branches before and after the point. As it is known, the Hopf bifurcation transform

the system from stable equilibria to stable oscillations, this type of Hopf bifurcation is called as supercritical Hopf. So that the section between Hopf point to LPC point, the oscillations are stable. The stability in limit cycle can be explained as the amplitude of oscillation converges to limit amplitude that calculated. The neutrally stable points are not a bifurcation points so that stability of the cycle does not change. After first fold point the LCO become unstable. Along the unstable line, oscillations can be attracted from random attractors which can cause failure in the structure due to excessive deformations. The unstable branch becomes stable once more after the second fold point.

There are two branch points on the line that lies between Hopf point and the first fold point. These branch points are connected each other. Along the green line that can be seen in Figure 6.2, three period doubling bifurcations, four fold bifurcations and two Neimark-Sacker (torus) bifurcations are observed.

At the period doubling bifurcation, the elliptic shape that is seen before period doubling changes its shape which is given in Figure 6.3. As mentioned in the part we explained the bifurcation types, the change in the parameter changes the trajectory of phase plane. One of the occurring conditions of period doubling is the possibility that frequency of the control surface can be defined with the integer multiplication of LCO frequency.
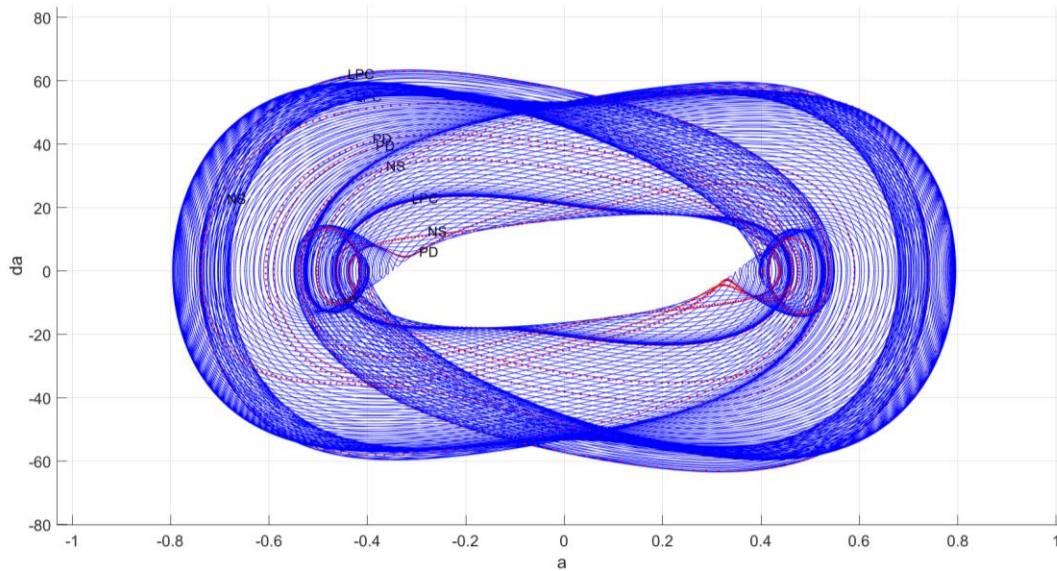
Figure 6.3. The phase plane change after period doubling

The normal form and first Lyapunov coefficients are used to decide the stability of the abovementioned bifurcations. The BPC points and Neimark-Sacker (torus) bifurcation points have the normal form coefficients less than zero so that after the bifurcations the limit cycle oscillations are still stable. The period doubling bifurcations are unstable due to positive normal form coefficient. The consequent period doubling makes the system more unstable, the cascade period doubling bifurcations could even cause chaos and destruction of the system.

The frequency change of the system with varying airspeed is given Figure 6.4. The frequency of the system and LCO amplitudes follows nearly same behavior. The similarity occurs due to the increasing rotation values makes the system more and more stiff which causes changes in the frequency of the limit cycle. The LCO frequency equals the flutter frequency at the beginning of the analysis however with the changing stiffness the frequency changes accordingly.
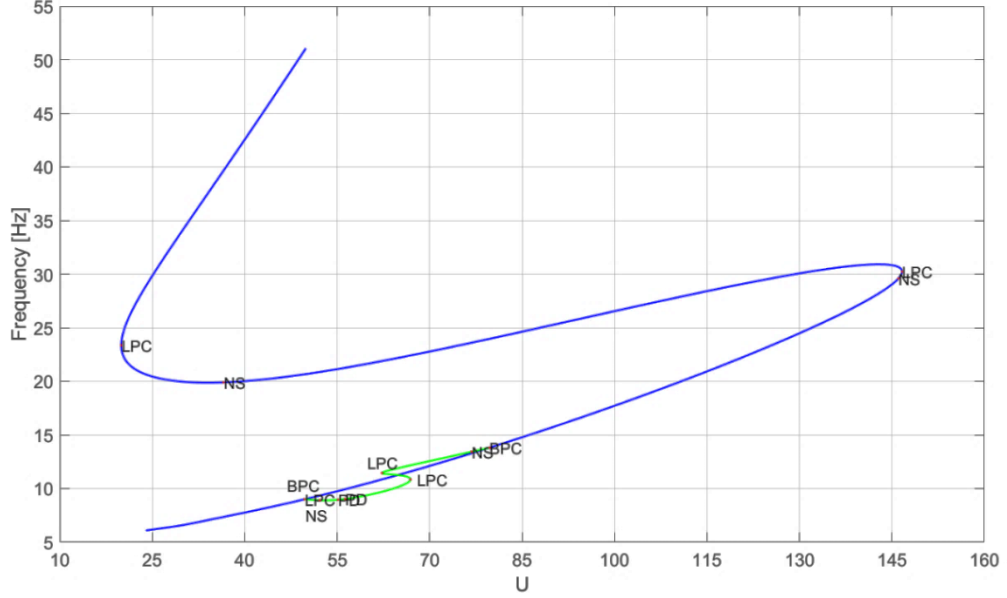
Figure 6.4. The response frequency with respect to airspeed for $K_{\alpha_3} = 373 \frac{Nm}{rad}$

6.1.2 Cubic Nonlinearity Analysis in Plunge Direction

The new AEOM with nonlinearity in plunge direction is given in Eq.6.3

$$\dot{x} = Qx + K_{h_3}qh^3 \qquad 6.3$$

where q is the forcing vector and given as follows

$$q = \begin{bmatrix} -(A + \rho B)^{-1} \begin{bmatrix} 1 \\ 0 \\ 0 \end{bmatrix} \\ 0_{9 \times 1} \end{bmatrix} \qquad 6.4$$

The results of introducing cubic stiffness into plunge direction differ from the pitch direction analysis. The Hopf point for the system is calculated at $U = 23.98 \ m/s$ that is the same Hopf point that was calculated in pitch direction analysis. The phase plane change of the system as the airspeed varying is given in Figure 6.5. For this analysis, the system shows subcritical Hopf bifurcation. The subcritical Hopf bifurcation is a dangerous phenomenon due to unstable nature. In supercritical Hopf bifurcation, the amplitudes of the limit cycle converge to a certain value as a result of being stable. However, in subcritical Hopf bifurcation the amplitude of limit cycle cannot be known and can be attracted by a random attractor.

59
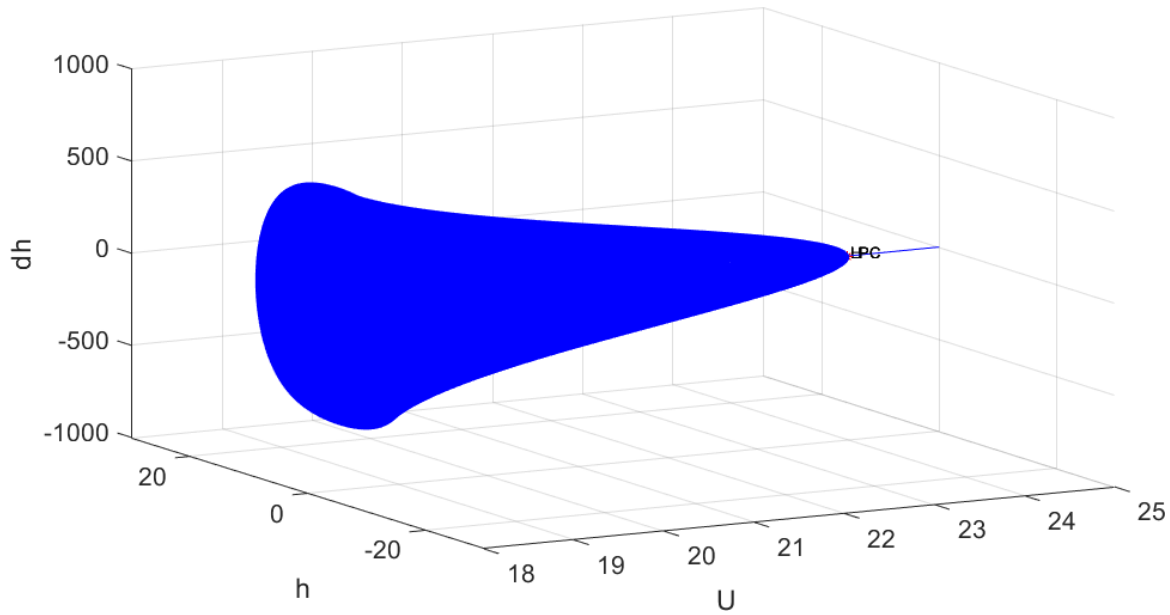
Figure 6.5. The cubic stiffness results for $K_{h_3} = 28.188\ Nm$

The bifurcation diagram of current analysis is given in the Figure 6.6. The results of current analysis show that the minimum initial conditions levels for LCO to be start. This situation shows also the importance of initial condition values for nonlinear systems.
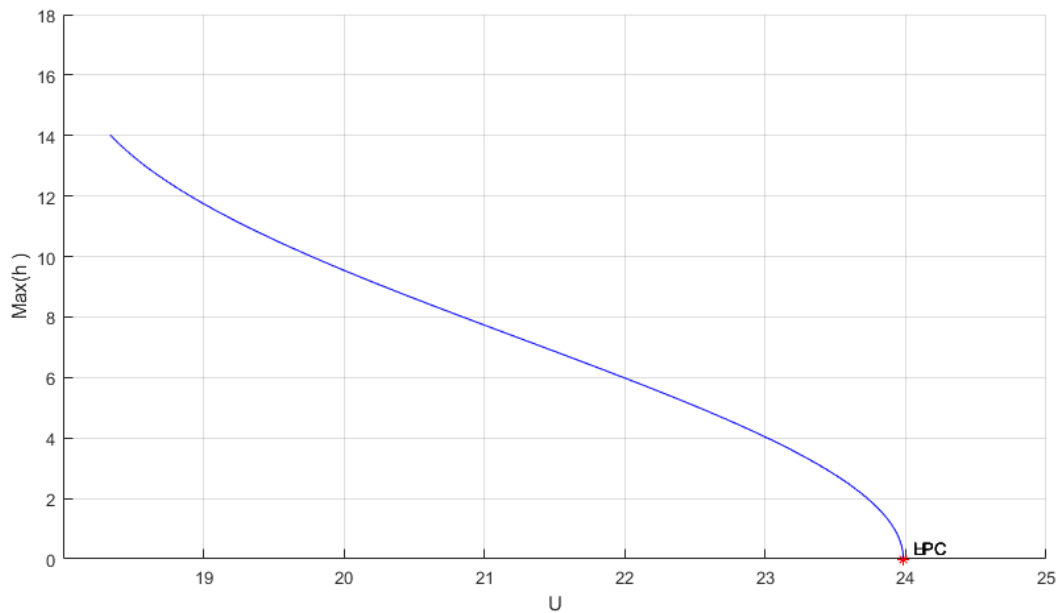

Figure 6.6. The bifurcation diagram for plunge response for $K_{h_3} = 28.188\ \dfrac{Nm}{rad}$

Higher initial condition values are required for the LCO to start at lower airspeeds which also cause higher frequency. The increasing frequency of plunge motion is getting closer to pitch frequency and more likely to create flutter mechanism. As mentioned before, the difference in frequency of two modes is an important factor that affects flutter behavior such as flutter speed and LCO occurrence.

Another aspect of the subcritical Hopf bifurcation is that it is frequency dependent. If the cubic stiffness high or low enough which means higher or lower frequency than the coupling require, the presence of LCO can be changed due to the frequency of the plunge mode will not be close to the coupled plunge mode anymore and cause to damp the oscillations. The frequency change of the oscillation is given in Figure 6.7.
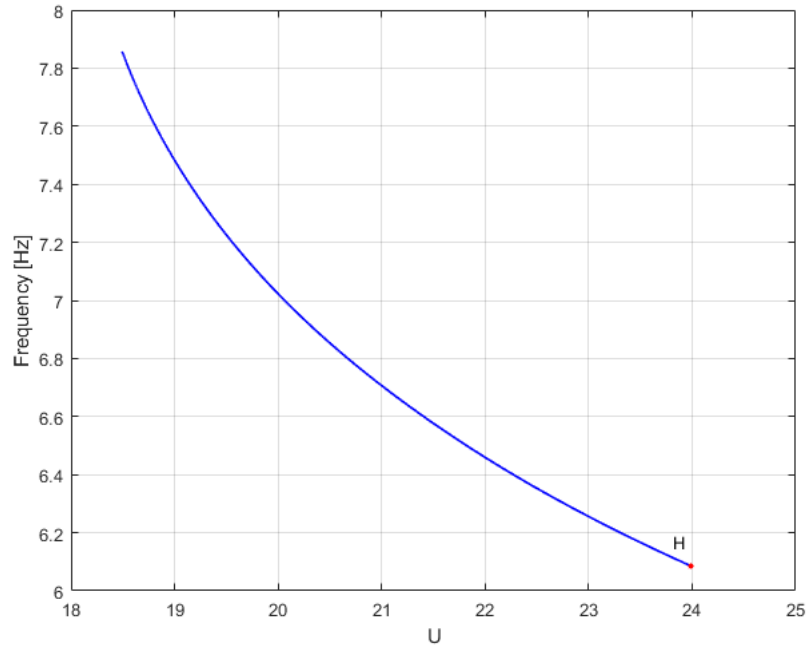

Figure 6.7. The frequency of limit cycle with respect to airspeed for $K_{h_3} = 28.188 \frac{Nm}{rad}$

6.1.3 Cubic Nonlinearity Analysis in Control Surface

The AEOM with nonlinearity in control surface is defined as given in Eq. 6.5

$$\dot{x} = Qx + K_{\alpha_3} q \beta^3 \qquad\qquad 6.5$$

where q is the forcing vector and given as follows

$$q = \begin{bmatrix} -(A + \rho B)^{-1} \begin{bmatrix} 0 \\ 0 \\ 1 \end{bmatrix} \\ \mathbf{0}_{9 \times 1} \end{bmatrix} \qquad 6.6$$

The effects of cubic stiffness on control surface differ from the aforementioned two analyses. In this analysis, the cubic stiffness does not have dominant control on the response of the airfoil in a manner of preventing divergent behavior because of the control surface mode does not make contribution to flutter mechanism. The phase plane change of the control surface response with increasing airspeed is given in Figure 6.8. As can be seen in this figure the response of the system increases rapidly with an increase in airspeed of about 0.25 m/s. At the airspeed $U = 23.98 \ m/s$, Hopf bifurcation is observed.
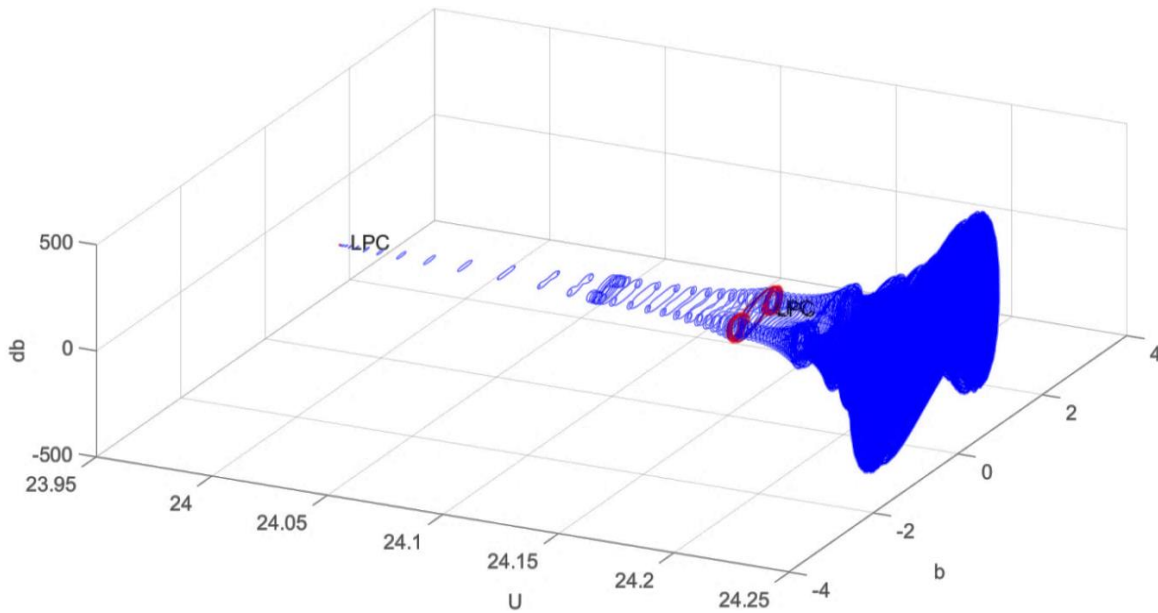
Figure 6.8. The cubic stiffness results for $K_{\beta_3} = 31.975 \ \frac{Nm}{rad}$

The bifurcation diagram of the system as the parameter U, airspeed changes is given in Figure 6.9. The MATCONT also find two fold points at the airspeed $U = 24.165 \ m/s$ and $U = 24.17 \ m/s$ at turning points. However as can be seen in bifurcation diagram, there are more turning points which could also be fold bifurcation. The MATCONT was not able to capture these bifurcations in this analysis which shows that the parameters that are chosen for the continuation analysis may cause to miss bifurcation points.
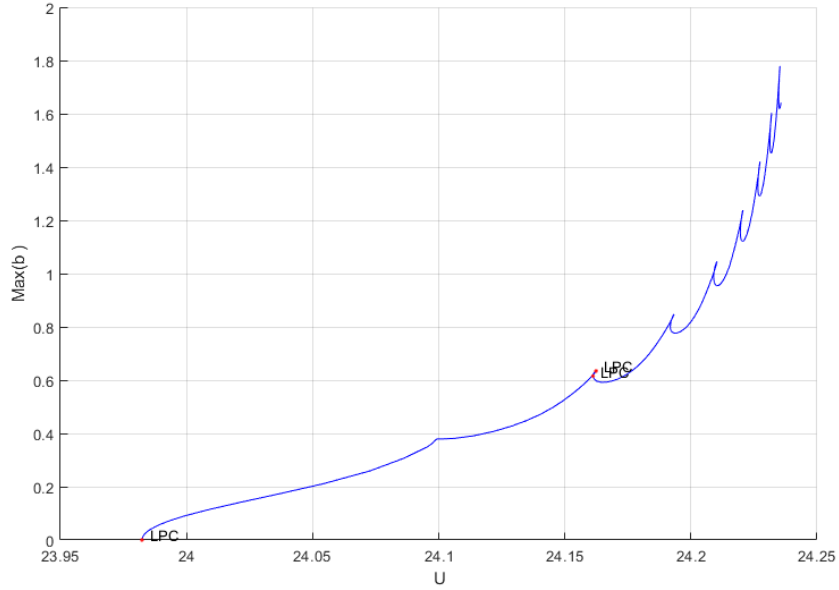
Figure 6.9. The bifurcation diagram for control surface response for $K_{\beta_3} = 31.975 \frac{Nm}{rad}$

The changes on the frequency with the varying airspeed can be seen in the Figure 6.10. The cubic stiffness in control surface direction does not cause a change in the fundamental frequency of LCO for the reason that stated at the beginning of this section.

Figure 6.10. The response frequency with respect to airspeed for $K_{\beta_3} = 31.975 \frac{Nm}{rad}$

6.2. Quadratic Damping Nonlinearity Analyses

The second nonlinearity that introduced into aeroelastic system is quadratic damping. The quadratic damping modeling is a more realistic damping method for modeling solid in a fluid. For the pitching degree of freedom, 0.1 and 1 quadratic damping coefficients are defined. The effects of damping on the system response for different levels of damping are investigated.
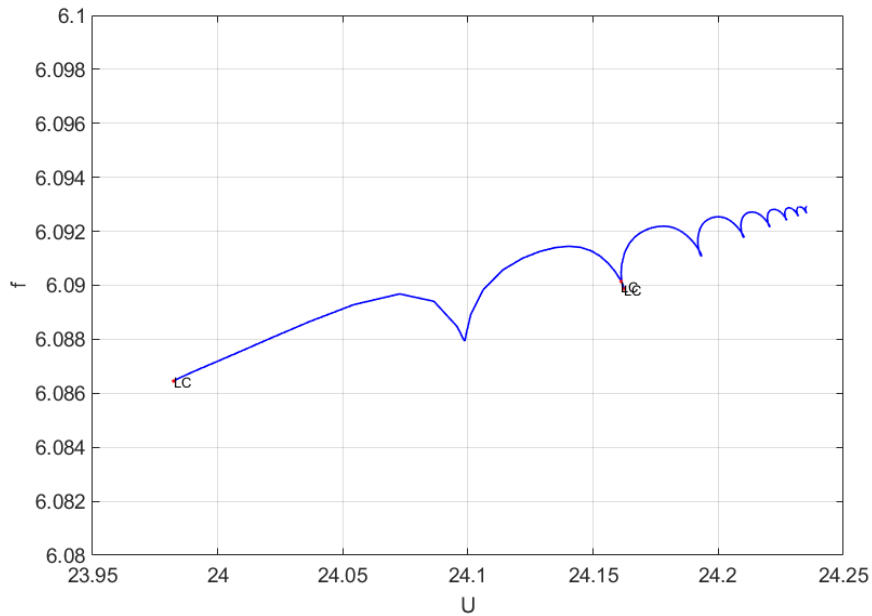
6.2.1 Quadratic Damping Nonlinearity Analyses in Pitch Direction

The new AEOM with nonlinearity in pitching direction is given in Eq. 6.7

$$\dot{x} = Qx + C_{\alpha_2}q\dot{\alpha}|\dot{\alpha}| \tag{6.7}$$

where q is the forcing vector and given as follows

$$q = \begin{bmatrix} -(A + \rho B)^{-1} \begin{bmatrix} 0 \\ 1 \\ 0 \end{bmatrix} \\ \mathbf{0}_{9\times1} \end{bmatrix} \tag{6.8}$$

In the first analysis, the quadratic coefficient $C_{\alpha_2} = 0.1$ is defined for the pitching direction. During the numerical continuation process, a Hopf and a fold (LPC) bifurcation is found. As in the Section 6.1.2, the system show subcritical Hopf bifurcation and the Hopf airspeed equals $U_H = 23.98\frac{m}{s}$. On the other hand, the fold bifurcation is encountered at the airspeed of $U = 21.91\frac{m}{s}$. The change of phase plane is given in Figure 6.11. As can be seen from this figure, the LCO characteristic of the system is preserved during the analysis.

64

Figure 6.11. The quadratic damping results for $C_{\alpha_2} = 0.1 \frac{N.m\ s}{rad}$

The bifurcation diagram for the pitching response is given in Figure 6.12. The section between Hopf bifurcation and fold bifurcation is unstable due to nature of subcritical Hopf bifurcation. The section became stable after fold bifurcation. In oscillated structures, the damping is a desired structural property. However, as can be seen in this example, the introduction of damping changes characteristics of the bifurcation and creates subcritical Hopf bifurcation and destabilizing effects for lower airspeed than Hopf speed.

The response frequency change of the system is given in Figure 6.13. As the airspeeds decreases from U_H, the frequency of the response starts to decrease as well. After the fold bifurcation, the decrease rate become slower and at a point the frequency of the response starts to increase.

Figure 6.12. The bifurcation diagram for pitching response for $C_{\alpha_2} = 0.1 \frac{N.m\,s}{rad}$
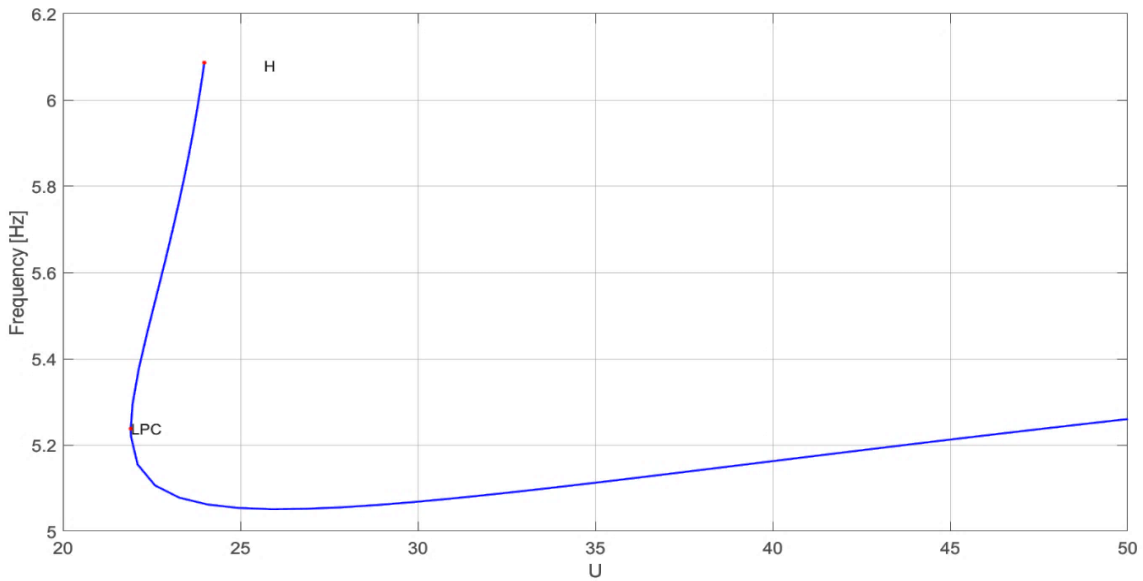
Figure 6.13. The response frequency with respect to airspeed for $C_{\alpha_2} = 0.1 \frac{N.m\,s}{rad}$

In the second analysis, quadratic damping coefficient $C_{\alpha_2} = 1 \frac{N.m\,s}{rad}$ is defined for pitching degree of freedom. The results of this analysis show same behavior with the previous

analysis except the levels of LCO amplitude. As the damping coefficient increases LCO amplitudes decreases. The phase plane change is given in Figure 6.14. The bifurcation diagram for pitching response is given in Figure 6.15.
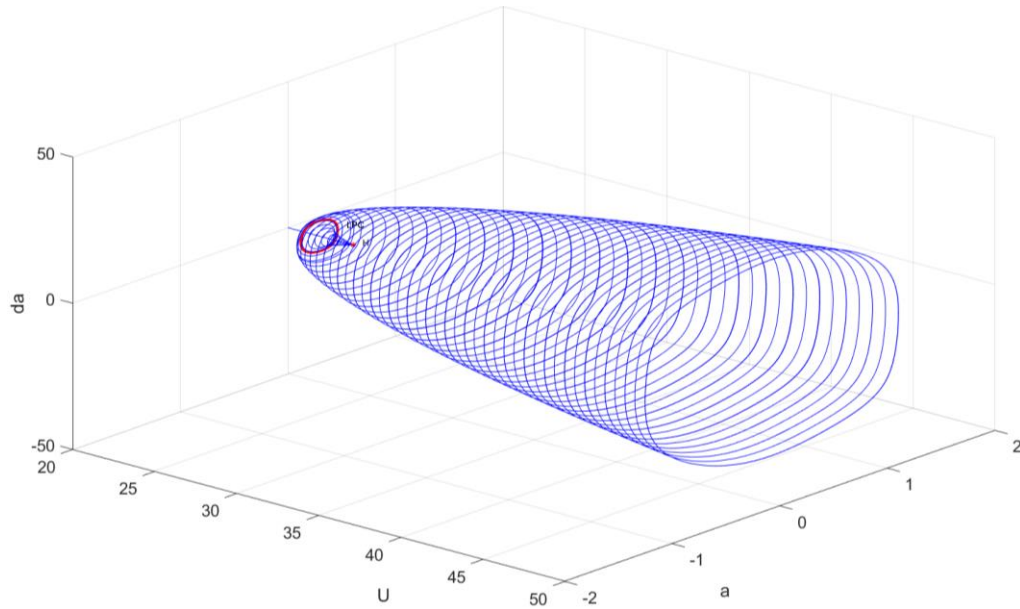

Figure 6.14. The quadratic damping results for $C_{\alpha_2} = 1 \frac{N.m\ s}{rad}$
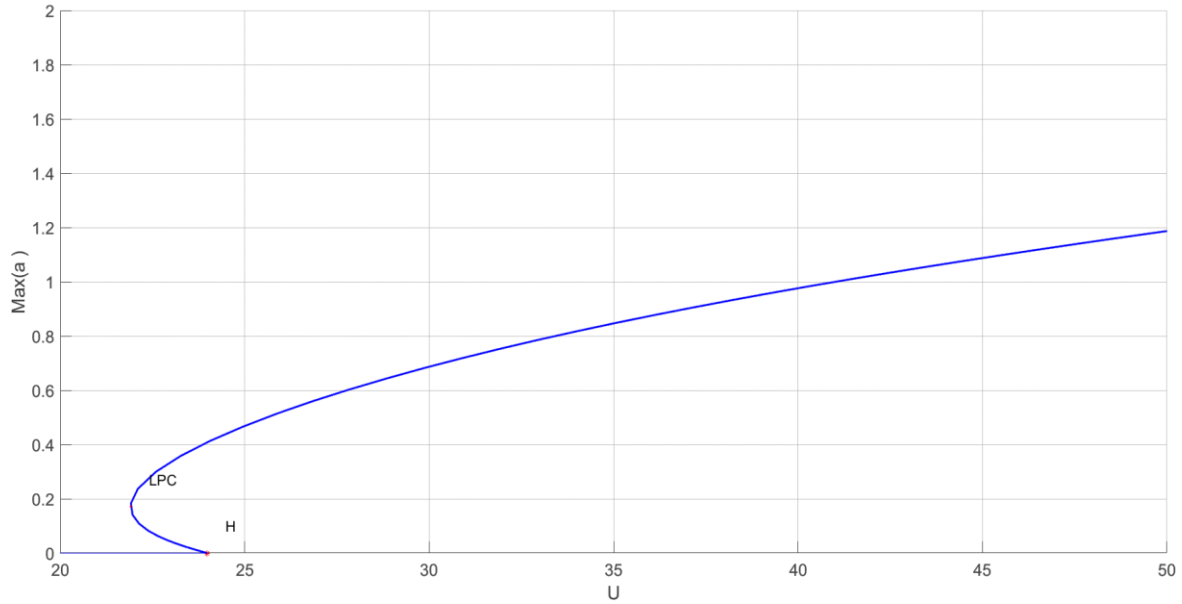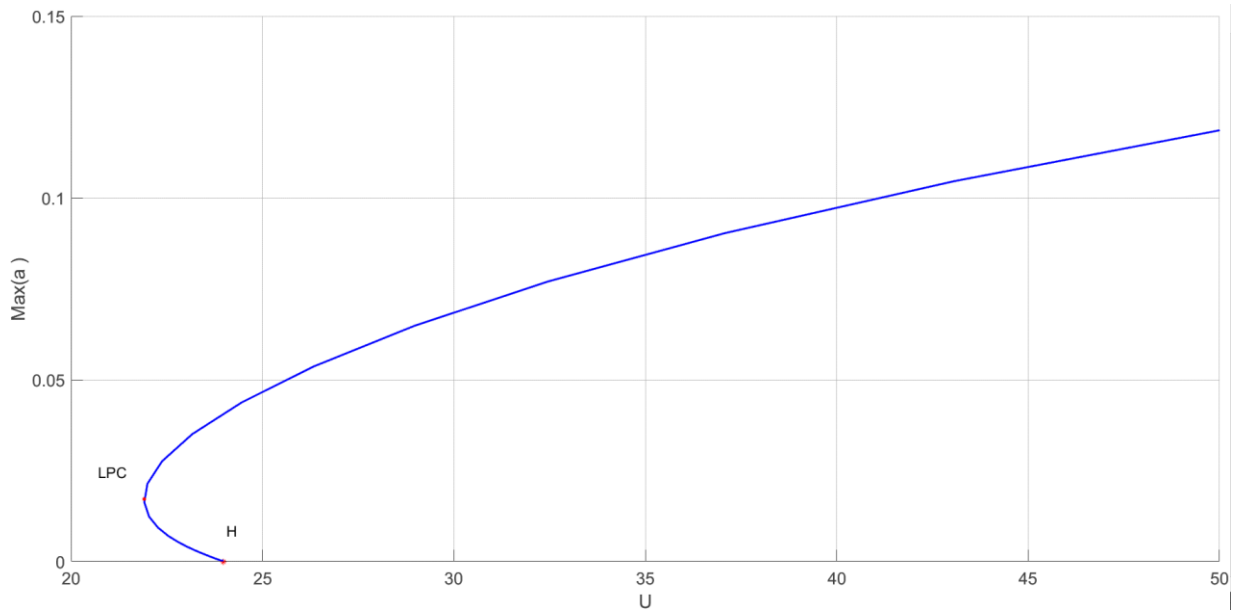

Figure 6.15. The bifurcation diagram for pitching response for $C_{\alpha_2} = 1 \frac{N.m\ s}{rad}$

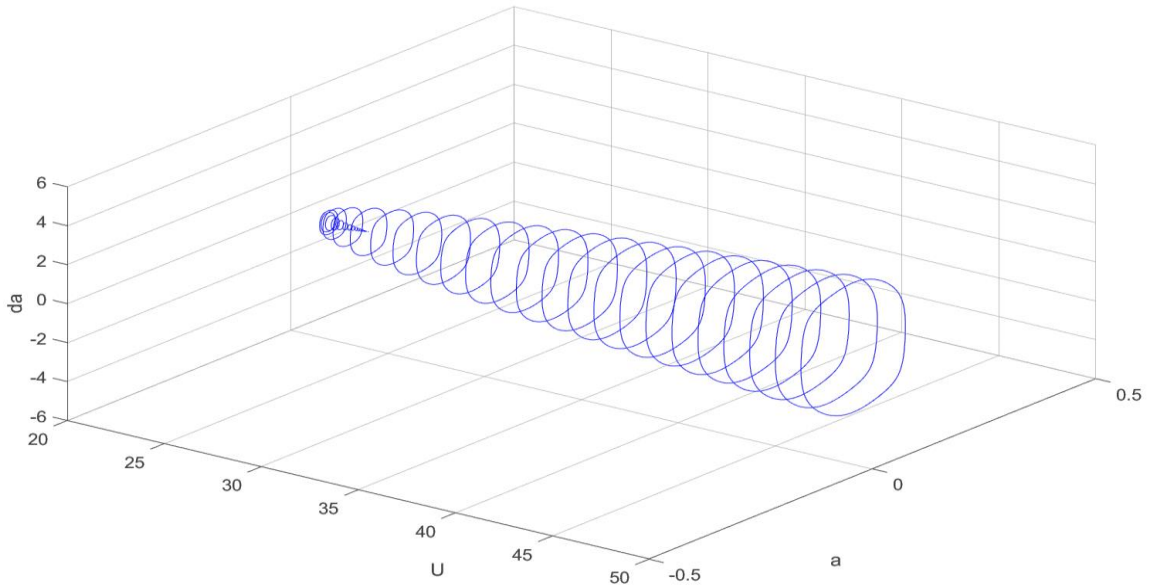The frequency of the response for quadratic damping coefficient $C_{\alpha_2} = 1$ is given in Figure 6.16. The frequency change is almost same for the analysis where $C_{\alpha_2} = 0.1$ is taken. As a result of these analyses, it is understood that the quadratic damping coefficient affect the amplitude of LCO but the frequencies and the behavior of the nonlinear system does not change.
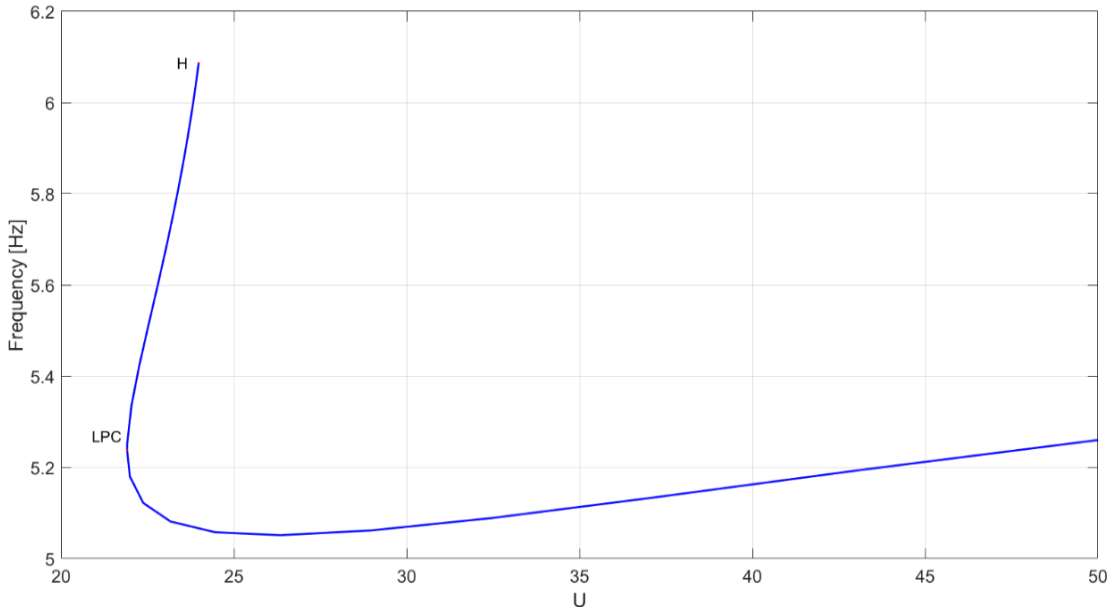
Figure 6.16. The response frequency with respect to airspeed for $C_{\alpha_2} = 1 \; \frac{N.m \; s}{rad}$

6.3. Free-Play Nonlinearity Analysis

The free-play occurs due to discontinuity in the stiffness. The main reasons of free-play are the mistolerances, manufacturing imperfections and gaps. The mathematical modeling of free play is given for moment calculation in Eq. 6.9 for torsional spring of pitching direction. The schematic representation of the free-play is given in Figure 6.17 for $\delta = 0.01 \; rad$. In this figure red dashed line belongs to mathematical representation of Eq. 6.9. On the other hand, the blue dashed line belongs to hyperbolic tangent method [46] for modeling piecewise linear free-play behavior. The mathematical model of mentioned method is given in 6.10.

$$M = \begin{cases} K(\alpha + \delta) & \alpha < -\delta \\ 0 & if \quad |\alpha| < \delta \\ K(\alpha - \delta) & \alpha > \delta \end{cases} \qquad 6.9$$

$$M = sign(\alpha)\sqrt{\left(\left(\frac{(g_1 + g_2)}{2}|\alpha| - \delta\right) + \frac{1}{2}((g_1 - g_2)^2(|\alpha| - \delta)^2 + 4g_1g_2\delta^2)\right)} \qquad 6.10$$

where δ, is the free-play angle, g_1 is the smoothness coefficient and g_2 is the stiffness value of linear system. As can be seen in Figure 6.17, the piecewise linear model and hyperbolic tangent model is almost coincident. As the derivative of piecewise linear model is not continuous, solving the nonlinear system equations with the hyperbolic tangent model approach will ease the numerical calculations.
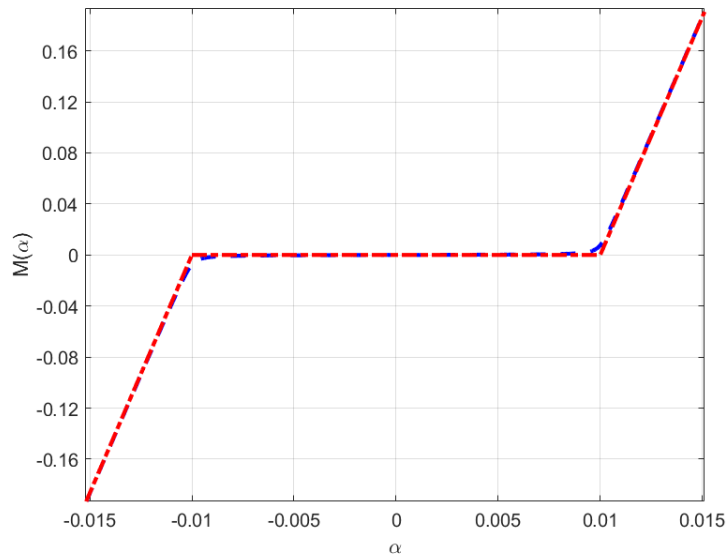
Figure 6.17. Comparison of piecewise linear and hyperbolic tangent models

It is understood that, introducing the nonlinearity on the control surface has nearly no impact on the behavior of the system. Therefore, free-play nonlinearity is introduced only in the pitching direction.

6.3.1 Free-Play Nonlinearity Analyzes in Pitching Direction

The mathematical model of the system is given in Eq. 6.11.

$$\dot{\boldsymbol{x}} = \boldsymbol{Q}\boldsymbol{x} + \boldsymbol{q}sign(\alpha)\sqrt{\left(\left(\frac{(g_1+g_2)}{2}|\alpha|-\delta\right)+\frac{1}{2}((g_1-g_2)^2(|\alpha|-\delta)^2+4g_1g_2\delta^2)\right)} \quad 6.11$$

where $\boldsymbol{q}$ is the forcing vector and given as follows

$$\boldsymbol{q} = \begin{bmatrix} -(\boldsymbol{A}+\rho\boldsymbol{B})^{-1}\begin{bmatrix} 0 \\ 1 \\ 0 \end{bmatrix} \\ \boldsymbol{0}_{9\times1} \end{bmatrix} \quad 6.12$$

The free-play analysis performed for the free play angle value of 0.01 rad. The corresponding value in degree is 0.573°. The phase plane change with respect to varying airspeed is given in Figure 6.18. There are two bifurcations along the LCO response curve. The first one is Hopf bifurcation which is encountered at the airspeed $U = 14.90\frac{m}{s}$ and the second bifurcation occur at the airspeed $U = 10.38\frac{m}{s}$ as a fold bifurcation.
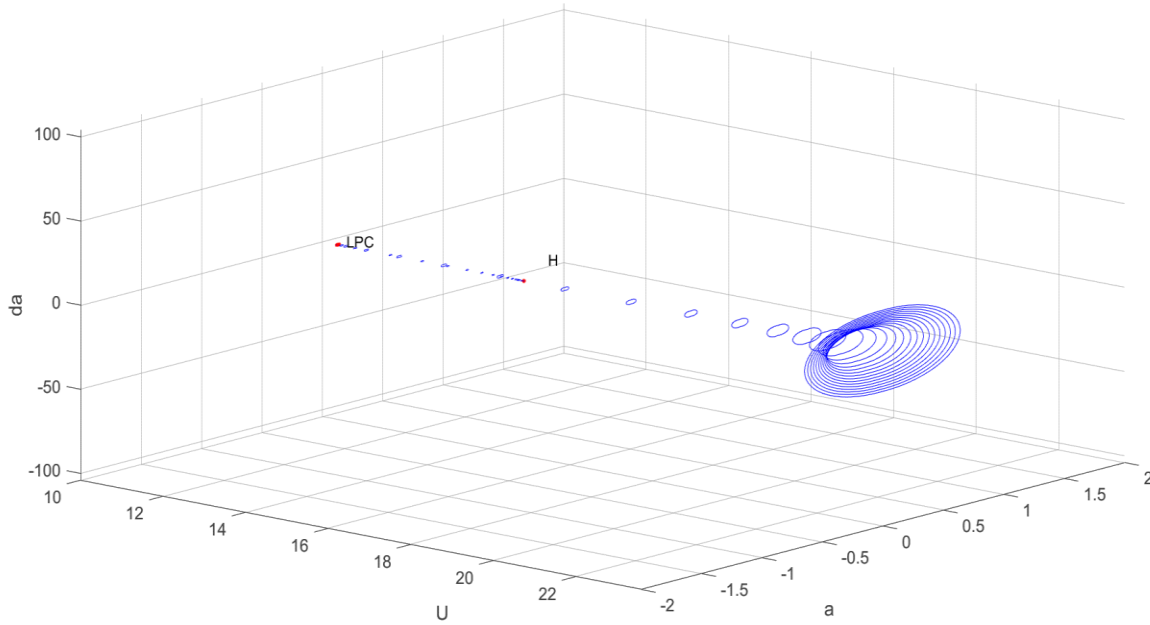
Figure 6.18. The quadratic damping results for $\delta_\alpha = 0.01\ rad$

The bifurcation diagram for pitching response of the system is given in Figure 6.19. The first Lyapunov of the Hopf bifurcation is positive which means the type of Hopf bifurcation is subcritical and the higher initial condition than the given amplitude between Hopf and fold bifurcation points cause unstable LCOs. The second bifurcation is fold bifurcation that transform unstable LCO behavior to stable LCO.
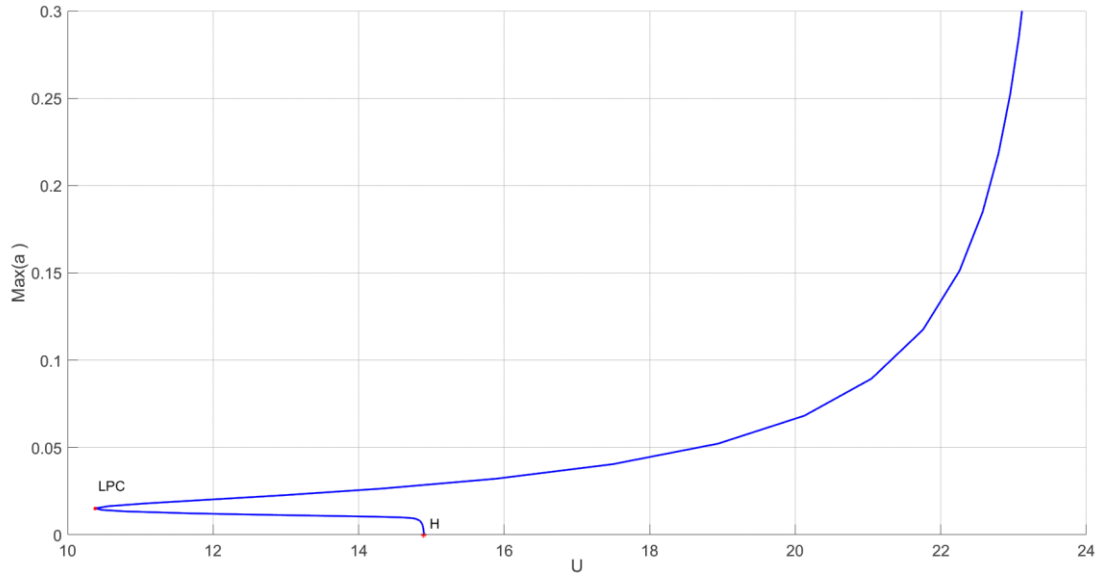
Figure 6.19. The bifurcation diagram for pitching response for $\delta_\alpha = 0.01 \, rad$

The frequency change of the system is given in Figure 6.20. As one can see, at the Hopf point the frequency of LCO equals the first natural frequency of the linear system due to there is no stiffness at the pitching direction. As the amplitude of the LCO oscillation increase, the amplitudes exceed the free-play angle and the system started to show reaction which causes increase on the frequency of pitch direction. For this reason, the frequency of the system increases as well. The flutter speed for the linear system was found at $U = 23.98 \frac{m}{s}$. As can be seen in Figure 6.19, as the airspeed approaches linear flutter speed, the LCO amplitude diverges.
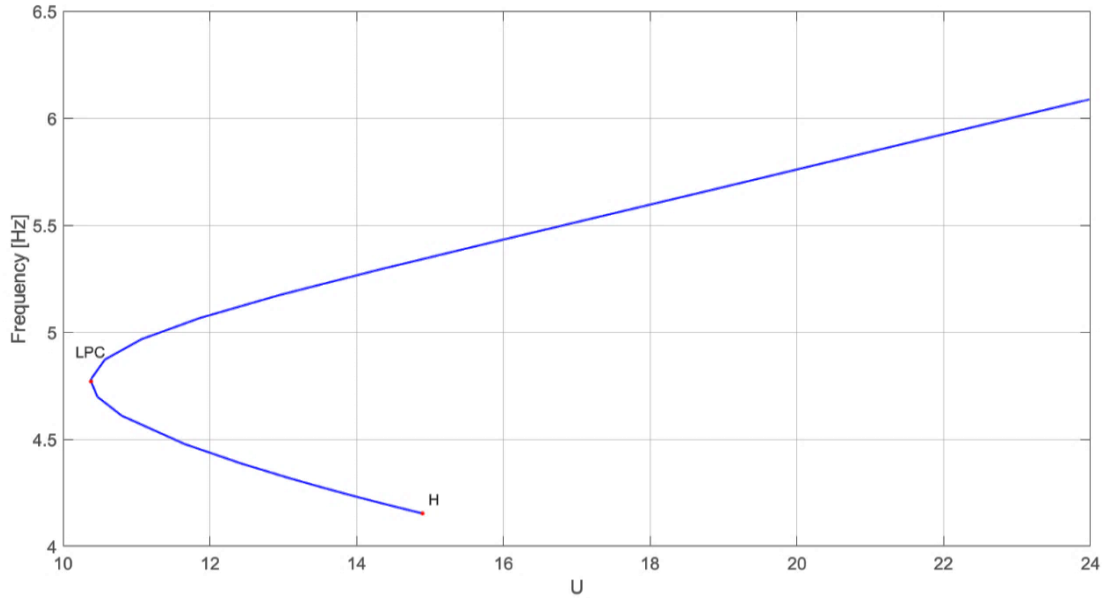
Figure 6.20. The response frequency with respect to airspeed for $\delta_\alpha = 0.01\ rad$

7. CONCLUSION AND FUTURE WORK

In this thesis, we derived equation of motion, unsteady aerodynamic force and moments, aeroelastic equation of motion for the 2D typical section with a control surface. The structural properties of the typical section are acquired from the article which was written by Conner et al [27]. The numerical analysis and ZAERO analysis are performed for the linear model to compare results with Conner's experimental results to check the consistency. The both analyses especially the numerical analysis is in good agreement with the experimental results. This agreement provides us to make assumption of numerical analysis of nonlinear system could be correlated with real systems. For the nonlinear calculations, MATCONT software is used which provides continuation analysis for discrete system instead of using time integration methods which are inefficient for highly nonlinear system.

In numerical analyzes the nonlinear structural elements such as cubic stiffness, quadratic damping and free-play nonlinearities were introduced to aeroelastic system. These nonlinearities affect the system in many different ways. First of all, the cubic stiffness that

72

defined in the pitching direction limit the oscillation limits and creates benign behavior and prevents the amplitudes to diverge. The introduction of cubic stiffness in plunge direction creates more dangerous behavior which is called as subcritical Hopf bifurcation. In the last cubic stiffness analysis, the nonlinearity was defined on the control surface of airfoil. The cubic nonlinearity on the control surface has nearly no effect on system response since it does not contribute to the flutter mechanism.

The quadratic damping nonlinearity creates more benign behavior and causes lower amplitude of oscillations. In quadratic damping analyses, it is seen that the value of the damping does not change frequency content. The subcritical Hopf bifurcation is also seen in these analyses. However, the subcritical range in these analyses is limited and does not occur elsewhere other than at the beginning of analyses.

Finally, in the free-play analysis, it is found that a system with free-play on the degree of freedom which creates flutter mechanism may experience LCO at the airspeed lower that linear flutter speed. It is found that as a result of subcritical Hopf bifurcation unstable LCO may be observed if the initial conditions higher than the response curve that is given in bifurcation diagram. Another finding of the analysis is that divergent behavior is observed as the air velocity approaches the linear flutter velocity. Once more it is understood that the underlying linear system has an important impact on the nonlinear system.

As a conclusion the degrees of freedom that creates the mode shapes which contribute to flutter mechanism has fundamental impact on the nonlinear system response. The underlying linear system defines the Hopf speed where LCOs arise. In this aspect it is important to say; even the nonlinear effects improve the system response in some cases, the structural properties of the linear system stands as one of the main factors that determine the system response in a way.

As a future work, the nonlinear effects on the aeroelastic system response for 3D model and higher Mach speeds will be studied. The achievements that are gained through this thesis will provide better understanding and judgment for the 3D model analyses.

8. REFERENCES

[1] U. Susuz, Aeroelastic Analysis of An Unmanned Aerial Vehicle,Master Thesis, Middle East Technical University Graduate School of Natural and Applied Science, Ankara, 2008.

[2] R. Vos and S. Farokhi, Intorduction to Transonic Aerodynamics, Springer, 2015.

[3] J. M. T. Thompson and H. B. Stewart, Nonlinear Dynamics and Chaos, Wiley, 1988.

[4] Y. Ning, W. Nan, Z. Xin and L. Wei, "Nonlinear flutter wind tunnel test and numerical analysis of folding fins with freeplay nonlinearities," Chinese Journal of Aeronautics, vol. 29, no. 1, p. 144–159, 2016.

[5] C. Nam, Y. Kim and T. A. Weisshaar, "Optimal sizing and placement of piezo actuators for active flutter suppression," 1995.

[6] D. W.J., "Introductory Survey," in Manuel on Aeroeasticity, Glasogow, AGARD, 1959, pp. 20-21.

[7] L. B.H.K., "Vertical tail buffeting of fighter aircraft," Progress in Aerospace Sciences, vol. 36, pp. 193-270, 2000.

[8] J. Drees, "Blade Twist, Droop Snoot, and Forward Spars," Wind Technology Journal, , vol. 1, no. 1, pp. 10-16, 1977.

[9] C. H. Gibbs-Smith, The Wright Brothers, A Brief Account of Their Work 1899-1911, Science Museum, 1987.

[10] C. G. H., " The Trials of the Langley Flying Machine at Hammondsport, N.Y.," Aeronautical journal, vol. 25, no. 132, p. 659–664, 1921.

[11] A. H. G. Fokker, The Flying Dutchman, 1931: Henry Holt and Co. .

[12] A. F. Baumhauer and C. Koning, "Oscillations of the Tail Plane and Body of an Aeroplane in Flight," National Advisory Commitee for Aeronautics, Amsterdam,

1916.

[13] H. Reissner, "Neuere probleme aus der flugzeugstatik," Z. für Flugtechnik und Motorluftschiffahrt, vol. 17, no. 7, pp. 137-146, 1926.

[14] H. Roxbee Cox and A. G. Pugsley, "Theory of Loss of Lateral Control Due to Wing Twisting," British ARC R&M, 1932.

[15] J. P. Giesing and W. P. S. B. Rodden, "Sears Function and Lifting Surface Theory for Hamnic Gust Fields," Journal of Aircraft, vol. 7, no. 3, pp. 252-255, 1970.

[16] M. W. Kehoe, "A Historical Overview of Flight Flutter Testing," NASA Technical Memorandum 4720, 1995.

[17] D. S. Woolston, H. L. Runyan and T. A. Byrdsong, "Some effects of system nonlinearities in the problem of aircraft flutter," National Advisory Committee for Aeronautics, Washington, 1955.

[18] S. SF, "An approximate analysis of nonlinear flutter problems.," An approximate analysis of nonlinear flutter problems, vol. 26, no. 1, p. 25–32, 1959.

[19] N. Kyrloff and N. Bogoliuboff, Introduction to Nonlinear Mechanics, Princeton: Princeton University Press, 1947.

[20] S. J. Price, B. H. K. Lee and H. Alighanbari, "Poststability behavior of a two-dimensional airfoil with a structural," Journal of Aircraft, vol. 31, no. 6, p. 1395–1401, 1994.

[21] T. Theodorsen, "General Theory of Aerodynamic Instability and the Mechanism of Flutter," National Advisory Commitee for Aeronautics, Washington, 1935.

[22] W. Eversman and A. Tewari, "Consistent rational-function approximation for unsteady aerodynamics," Journal of Aircraft, vol. 28, no. 9, pp. 545-552, 1991.

[23] D. Woolston, H. Runyan and R. Andews, "An investigation of effects of certain types of structural nonlinearities on wing and control surface flutter," Journal of Aeronautical Science, vol. 24, no. 1, pp. 57-63, 1957.

[24] Z. Yang and Zhao, "Analysis of limit cycle flutter of an airfoil in incompressible flow," Journal of Sound and Vibration, vol. 123, no. 1, pp. 1-13, 1988.

[25] S. McIntosh Jr., R. Reed Jr and W. Rodden, "Experimental and theoretical study of nonlinear flutter," Journal of Aircraft, vol. 18, pp. 1057-1063, 1981.

[26] K. Chung, C. Chan and B. Lee, "Bifurcation analysis of two-degree-of-freedom aeroelasticy system withe freeplay structural nonlinearity by a perturbation-incremental method," Journal of Sound and Vibration , vol. 299, pp. 520-539, 2007.

[27] M. D. Conner, D. M. Tang and E. H. D. a. L. Virgin, "Nonlinear Behavior of a Typical Airfoil Section with Control Surface Freeplay : A Numerical and Experimental Study," Journal of Fluids and Structures, vol. 11, pp. 89-109, 1997.

[28] S. Irani, H. Sarrafzadeh and M. R. Amoozgar, "Bifurcation in a 3-DOF Airfoil with Cubic Structural Nonlinearity," Chinese Journal of Aeronautics, vol. 24, pp. 265-278, 2011.

[29] M. Karpel and D. Raveh, "Fictitious Mass Element in Structural Dynamics," AIAA, vol. 34, no. 3, pp. 607-615, 1996.

[30] D. Lee and P. Chen, "Nonlinear Aeroelastic Studies on Folding Wing Configuration with Free-play Hinge Nonlinearity," in AIAA/ASME/ASCE/AHS/ASC Structures, Structural Dynamics, and Materials Conference, New Port, 2006.

[31] Z. Zhang, P. Chen, X. Wang and M. P. Mignolet, "Nonlinear Aerodynamics and Nonlinear Structures Interaction For F-16 Limit Cycle Oscillation Prediction," in 15th Dynamics Specialists Conference, San Diego, 2016.

[32] D. O. Fearnow, "Investigation of the structural damping of a full-scale airplane wing," in NACA, Washington, 1952.

[33] T. Dossogne, N. J.P., C. Grappasonni, G. Kerschen, B. Peeter, J. Debille and M. a. S. J. Vaes, "Nonlinear Ground Vibration Identification of an F-16 Aircraft - Part II:Understanding Nonlinear Behaviour in Aerospace Structure Using Sine-Sweep Testing," in IFASD, Saint Petersburg, 2015.

[34] M. B. Dalmış, Flutter Characteristics of Plate Like Structures, Master Thesis, Middle East Technical University Graduate School of Natural and Applied Science, Ankara, 2014.

[35] T. B. Balevi, Flutter Analysis and Simulated Flutter Test Of Wings, Master Thesis, Middle East Technical Univerity Graduate School of Natural and Applied Science, Ankara, 2012.

[36] E. N. Yıldız, Aeroelastic Stability Prediction Using Flutter Flight Test Data, Doctoral Thesis, Middle East Technical University Graduate School of Natural and Applied Science, Ankara, 2007.

[37] B. Ertürk, Effects of design parameters on the aeroelastic performance of a cruise missile wing, Master Thesis, Middle East Technical University Graduate School of Natural and Applied Science, Ankara, 2019.

[38] M. G.D., Theory of Lift, Introductionary Computational Aerodynamics in MATLAB/Octave, John Wiley & Sons Ltd, 2012.

[39] a. W. G. Y. K. H. M. S. A. Dhooge, "New features of the software MatCont for bifurcation analysis of dynamical systems.," MCMDS, vol. Vol. 14, no. No. 2, pp. pp 147-175, 2008.

[40] R. Seydel, Practical Bifurcation and Stability Analysis, Köln: Springer, 2010.

[41] G. Dimitriadis, Introduction to Nonlinear Aeroelasticity, 1st ed., Chichester, West Sussex: John Wiley & Sons, Inc., 2017.

[42] "Scholarpedia," [Online]. Available: http://www.scholarpedia.org/article/MATCONT. [Accessed 6 August 2021].

[43] Z. Technology, "ZAERO Basic Training," Arizona, 2020.

[44] Z. Technology, Te, Arizona: Zona Technology, 2017.

[45] W. R. a. B. E. Rodden, "Aeroelastic Addition to NASTRAN," NASA CR, 1979.

[46] D. C. Asjes, A. Diwadkar, U. Vaidya and A. Kelkar, "Development and System Analysis of a Two-Dimensional Rotational Freeplay Nonlinearity Model," Journal of Aircraft, vol. 53, no. 3, pp. 860-864, 2016.

APPENDIX

APPENDIX 1 – Explicit Forms of Structural and Aerodynamic Matrices

$$A = \begin{bmatrix} m & S & S_\beta \\ S & I_\alpha & I_{\alpha\beta} \\ S_\beta & I_{\alpha\beta} & I_\beta \end{bmatrix}$$

$$E = \begin{bmatrix} K_h & 0 & 0 \\ 0 & K_\alpha & 0 \\ 0 & 0 & K_\beta \end{bmatrix}$$

$$C = \begin{bmatrix} C_h & 0 & 0 \\ 0 & C_\alpha & 0 \\ 0 & 0 & C_\beta \end{bmatrix}$$

$$B = b^2 \begin{bmatrix} \pi & -\pi a b & -T_1 b \\ -\pi a b & \pi b^2 \left(\frac{1}{8} + a^2 \right) & -(T_7 + (c_h - a)T_1)b^2 \\ -T_1 b & 2T_{13}b^2 & -T_3 b^2/\pi \end{bmatrix}$$

$$D = D_1 + \Phi(0)D_2$$

$$\Phi(0) = 1 - \Psi_1 - \Psi_2$$

$$D_1 = b^2 \begin{bmatrix} 0 & \pi & -T_4 \\ 0 & \pi\left(\frac{1}{2} - a\right)b & \left(T_1 - T_8 - (c_h - a)T_4 + \frac{T_{11}}{2}\right)b \\ 0 & \left(-2T_9 - T_1 + T_4\left(a - \frac{1}{2}\right)\right)b & -T_4 T_{11} b/2\pi \end{bmatrix}$$

$$D_2 = \begin{bmatrix} 2\pi b & 2\pi b^2\left(\frac{1}{2} - a\right) & b^2 T_{11} \\ -2\pi b^2\left(a + \frac{1}{2}\right) & -2\pi b^2\left(a + \frac{1}{2}\right)\left(\frac{1}{2} - a\right) & -b^3\left(a + \frac{1}{2}\right)T_{11} \\ b^2 T_{12} & b^3 T_{12}\left(\frac{1}{2} - a\right) & b^3 T_{12} T_{11}/2\pi \end{bmatrix}$$

$$F = F_1 + \Phi(0)F_2 + \Xi F_3$$

$$\Xi = \frac{\Psi_1 \varepsilon_1}{b} + \frac{\Psi_2 \varepsilon_2}{b}$$

$$F_1 = b^2 \begin{bmatrix} 0 & 0 & 0 \\ 0 & 0 & (T_4 + T_{10}) \\ 0 & 0 & (T_5 - T_4 T_{10})/\pi \end{bmatrix}$$

$$F_2 = \begin{bmatrix} 0 & 2\pi b & 2b T_{10} \\ 0 & -2\pi b^2\left(a + \frac{1}{2}\right) & -2b^2\left(a + \frac{1}{2}\right)T_{10} \\ 0 & b^2 T_{12} & b^2 T_{12} T_{10}/\pi \end{bmatrix}$$

$$F_3 = D_2$$

$$W = \begin{bmatrix} 2\pi b W_0 & -2\pi b^2\left(a + {}^1\!/_2\right)W_0 & b^2 T_{12} W_0 \end{bmatrix}$$

$$W_0 = \begin{bmatrix} \Psi_1\left({}^{\varepsilon_1}\!/_b\right)^2 \\[2mm] \Psi_2\left({}^{\varepsilon_2}\!/_b\right)^2 \\[2mm] \Psi_1\varepsilon_1\left(1 - \varepsilon_1\left({}^1\!/_2 - a\right)\right)\Big/_b \\[3mm] \Psi_2\varepsilon_2\left(1 - \varepsilon_2\left({}^1\!/_2 - a\right)\right)\Big/_b \\[3mm] \Psi_1\varepsilon_1\left(T_{10} - {}^{\varepsilon_1 T_{11}}\!/_2\right)\Big/_{\pi b} \\[4mm] \Psi_2\varepsilon_2\left(T_{10} - {}^{\varepsilon_2 T_{11}}\!/_2\right)\Big/_{\pi b} \end{bmatrix}$$

$$W_1 = \begin{bmatrix} 1 & 0 & 0 \\ 1 & 0 & 0 \\ 0 & 1 & 0 \\ 0 & 1 & 0 \\ 0 & 0 & 1 \\ 0 & 0 & 1 \end{bmatrix}$$

$$W_2 = \begin{bmatrix} -{}^{\varepsilon_1}\!/_b & 0 & 0 & 0 & 0 & 0 \\ 0 & -{}^{\varepsilon_2}\!/_b & 0 & 0 & 0 & 0 \\ 0 & 0 & -{}^{\varepsilon_1}\!/_b & 0 & 0 & 0 \\ 0 & 0 & 0 & -{}^{\varepsilon_2}\!/_b & 0 & 0 \\ 0 & 0 & 0 & 0 & -{}^{\varepsilon_1}\!/_b & 0 \\ 0 & 0 & 0 & 0 & 0 & -{}^{\varepsilon_2}\!/_b \end{bmatrix}$$